

SPECIAL ISSUE ARTICLE

Denudation variability of the Sila Massif upland (Italy) from decades to millennia using ^{10}Be and $^{239+240}\text{Pu}$ Gerald Raab¹  | Fabio Scarciglia² | Kevin Norton³ | Dennis Dahms⁴ | Dagmar Brandová¹ | Raquel de Castro Portes¹ | Marcus Christl⁵ | Michael E. Ketterer⁶ | Annina Ruppli¹ | Markus Egli¹¹Department of Geography, University of Zurich, Zurich, Switzerland²Department of Biology, Ecology and Earth Sciences (DiBEST), University of Calabria, Arcavacata di Rende, Italy³School of Geography, Environment and Earth Sciences, Victoria University of Wellington, Wellington, New Zealand⁴Department of Geography, University of Northern Iowa, Cedar Falls, Iowa⁵Department of Physics, ETH Zurich, Zurich, Switzerland⁶Chemistry and Biochemistry, Northern Arizona University, Flagstaff, Arizona**Correspondence**

Gerald Raab, Department of Geography, University of Zurich, Winterthurerstrasse 190, 8057 Zurich, Switzerland.

Email: gerald.raab@geo.uzh.ch

Funding information

Schweizerischer Nationalfonds zur Förderung der Wissenschaftlichen Forschung, Grant/Award Number: 200021_162338/1 IZK0Z2_147421 IZK0Z2_170715/1; SNSF grant for a Short Research Visit, Grant/Award Number: IZK0Z2_147421; Royal Society Te Apārangi Rutherford Discovery Fellowship; SNSF Visiting International Fellowship, Grant/Award Number: IZK0Z2_170715/1

Abstract

Landscapes and soils evolve in non-linear ways over millennia. Current knowledge is incomplete as only average denudation (or erosion) rates are normally estimated, neglecting the temporal discontinuities of these processes. The determination of regressive and progressive phases of soil evolution is important to our understanding of how soils and landscapes respond to environmental changes. The Sila Massif (Italy) provides a well-defined geomorphological and geological setting to unravel temporal variations in soil redistribution rates. We used a combination of in situ cosmogenic radionuclide measurements (^{10}Be) along top (residual rock) height profiles, coupled with fallout radionuclides ($^{239+240}\text{Pu}$) in soils, to model soil denudation rates over the last 100 ka. We measured rates prior to the Last Glacial Maximum (LGM) of $\leq 30 \text{ t km}^{-2} \text{ year}^{-1}$ ($\sim 0.036 \text{ mm year}^{-1}$). Following the LGM, during the transition from the Pleistocene to the Holocene, these rates increased to $\sim 150\text{--}200 \text{ t km}^{-2} \text{ year}^{-1}$ and appeared to be above soil production rates, causing regressive soil evolution. For the last ~ 50 years, we even describe erosion rates of $\geq 1,000 \text{ t km}^{-2} \text{ year}^{-1}$ ($\sim 1.23 \text{ mm year}^{-1}$) and consider human impact as the decisive factor for this development. Consequently, the natural soil production rates cannot cope with the current erosion rates. Thus, a distinct regressive phase of soil formation exists, which will give rise to shallowing of soils over time. Overall, our multimethod approach traced denudation and erosion histories over geologic and human timescales and made a new archive to soil science and geomorphology accessible.

KEYWORDS

cosmogenic nuclides, fallout radionuclides, landscape evolution, soil erosion rates, soil formation

1 | INTRODUCTION

Earth's surface landscapes are known to form in complex and non-linear ways over thousands of years—this is particularly the case for soils. In a coevolutional model, soil formation is regarded to be discontinuous over time and conceptualised by 'progressive' or 'regressive' process groups (Johnson & Watson-Steger, 1987; Sommer, Gerke, & Deumlich, 2008) that are caused by changing environmental conditions. Periods with dominantly progressive processes (e.g., soil

deepening and weathering) alternate with periods with dominantly regressive processes (e.g., erosion) due to fast and substantial changes in drivers. Soils can only form if the rate of their production is higher than the rate of soil loss. Soil formation (F_{soil}) can be expressed by

$$F_{\text{soil}} = P_{\text{soil}} - D_{\text{soil}}, \quad (1)$$

where P_{soil} is the soil production and D_{soil} the soil denudation. Progressive phases occur when soil production is greater than soil denudation,

and regressive phases occur when soil denudation rates are greater than soil production. Denudation fluxes (D) consist of chemical weathering fluxes (W) and physical erosion fluxes (E):

$$D_{soil} = W_{soil} + E_{soil}, \quad (2)$$

where W_{soil} is the chemical weathering fluxes (leaching losses) and E_{soil} is the soil erosion. Chemical and physical weathering and mineral transformation contribute to progressive soil formation, whereas strong erosion leads to regressive development and thereby to surface denudation. Often, soil erosion is almost equal to denudation. Dixon and von Blanckenburg (2012), Reeves and Rothman (2014), and several others have demonstrated that soil erosion is the driving force

for denudation in agricultural landscapes and hill country. In steep mountainous terrain, mass wasting dominates. Soil erosion (catchment-wide to profile-related data) is mostly in the range of 0.5–0.9 D_{soil} (Dixon & von Blanckenburg, 2012):

$$0.5 \cdot D_{soil} \leq E_{soil} \leq 0.9 \cdot D_{soil}. \quad (3)$$

Changes in soil-forming factors can be very abrupt across space and time in mountain landscapes, either because of catastrophic natural events or by human influences (e.g., land use changes and agriculture intensification; Egli & Poulencard, 2016). The concern about soil erosion increases worldwide. Also in Europe (Figure 1a), there is a need to understand erosion processes to establish mitigation measures. This

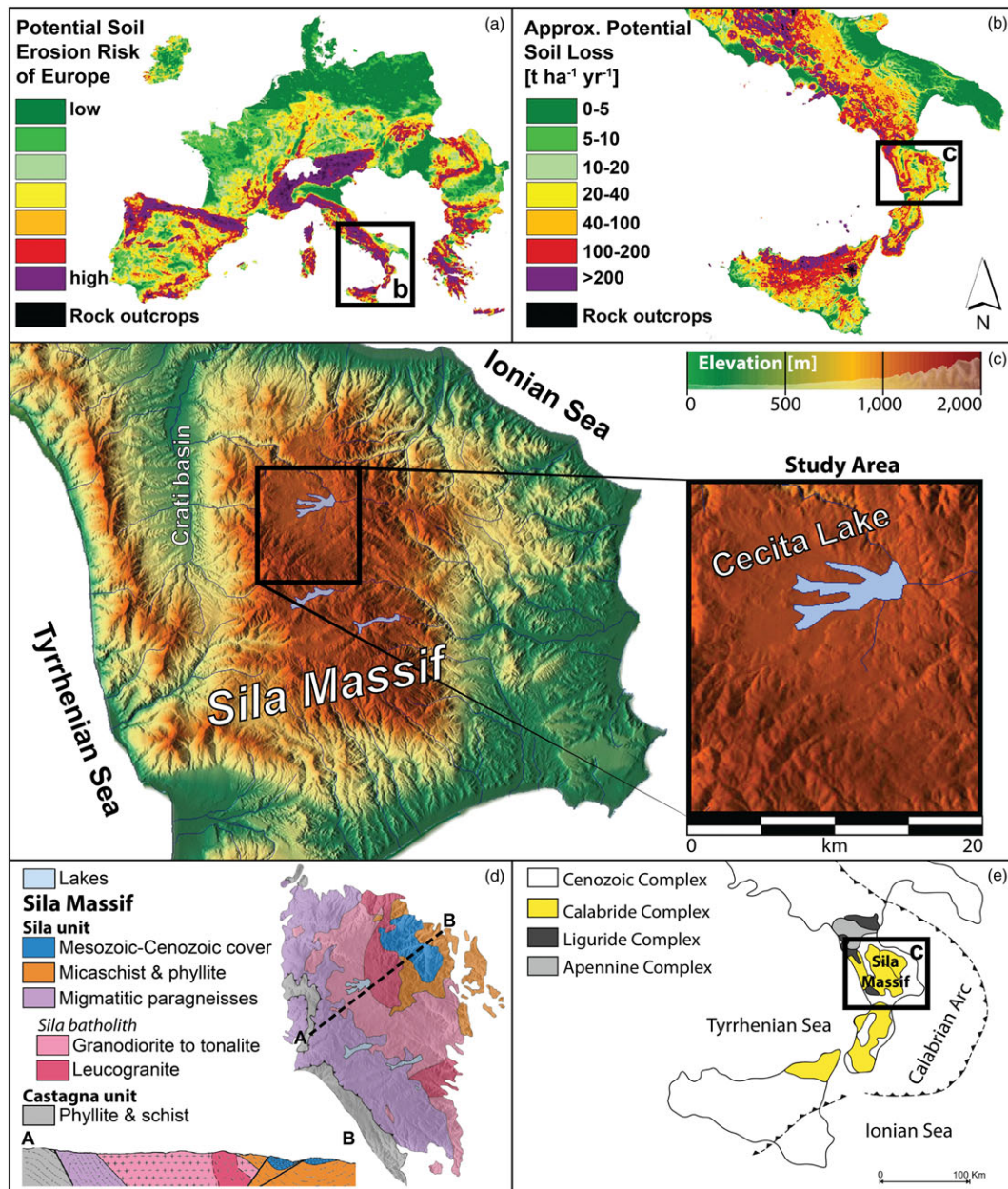


FIGURE 1 (a) Potential soil erosion risk map of Europe (black square: southern Italy), modified after van der Knijff, Jones, and Montanarella (2000). (b) Approximate potential soil loss in southern Italy (van der Knijff, Jones, & Montanarella, 1999). (c) Topographic map of the Sila Massif and the study area near the Cecita Lake, based on data of the Geoportale Nazionale (Ministero dell'Ambiente, Italy). (d) Geological overview of the Sila Massif based on von Eynatten, Tolosana-Delgado, Karius, Bachmann, and Caracciolo (2015) and Liotta et al. (2008). (e) Geological framework of the Sila Massif after Vespasiano et al. (2015) [Colour figure can be viewed at wileyonlinelibrary.com]

is particularly the case for countries such as Italy with a large proportion of mountainous and landscapes having steep slopes (Figure 1b). Several recent studies attempt to compare erosion rates over various time periods in order to estimate rates of various geomorphic processes (e.g., Bellin, Vanacker, & Kubik, 2014; Kirchner et al., 2001). These studies, however, often used catchment-wide approaches (e.g., Bartley, Croke, Brainbridge, Austin, & Kuhnert, 2015; Ibbeken & Schleyer, 1991) and, thus, cannot distinguish soil erosion from denudation as a general degradation process, which is a combination of (soil and rock) erosion, weathering, and mass wasting. Qualitative or quantitative estimates of erosion rates over different timescales have been reported for river sediment yields (Bartley et al., 2015; Kirchner et al., 2001), for lake and marine sedimentation (Mourier, Poulencard, Carcaillet, & Williamson, 2010), and for speleothem growth rates (Clift, Wan, & Blusztajn, 2014). Under specific conditions, the quantification of soil erosion over a few millennia has been possible to high precision through the use of lake sediment records (Bajard et al., 2017).

Up to now, deciphering the temporal development of soil erosion or denudation (and related soil production) over millennia has been difficult (Bajard et al., 2017; Boardman & Poesen, 2007; Poesen, 2018), and our knowledge in this field remains incomplete and fragmented. Neglecting the fact that soil erosion processes are discontinuous over time weakens the understanding of a modern degradation mechanism that has a huge economic and environmental impact (Pimentel, 2006).

Soil denudation and erosion are driven by tectonic activity, local geology, surface topography, climate, and anthropogenic and biotic activities (Smithson et al., 2008). In order to estimate soil erosion over longer time periods, an area has to be selected that predominantly traces soil erosion and not mass wasting or rock (or saprolite) erosion. Thus, archives have to be investigated that optimally preserve this temporal information. Intense erosion- and denudation-affected landscapes can be identified by the presence of boulder fields or 'tor and bornhardt' landforms (Migoń, 2013; Twidale, 2002). These landscapes usually exhibit tower-like or dome-shaped, often castellated residual rocks (tors) that appear to grow from surrounding gentle landforms. We hypothesise that tors are a key for deciphering the evolution of surface lowering rates over time. Where surface lowering is primarily linked to a decrease in soil volume, soil erosion or denudation rates can be deduced. Rock tors (linked to the bedrock) and boulders (detached from the bedrock) usually have a higher physical resistance than the surrounding more easily weatherable (saprolite) material. In an eroding landscape, tors consequently progressively extend above their surrounding landscape surfaces. The rate at which a tor extends further above its landscape is an indicator of the rate of (soil) denudation of the surrounding surface.

Through the use of cosmogenic radionuclide techniques, the exposure of tors and boulders can be dated. Several authors estimated the exposure ages of such landforms. In most cases, however, only samples at the top of tors/boulders were analysed (e.g., Bierman & Caffee, 2001; Darmody et al., 2008; Gunnell et al., 2013). A more detailed sampling design has very rarely been applied (Heimsath, Chappell, Dietrich, Nishiizumi, & Finkel, 2001; Wakasa, Matsuzaki, Tanaka, & Matsukura, 2006). The ^{10}Be exposure ages obtained from

the vertical profile of tor surfaces should allow us to determine their exhumation rates and consequently to calculate surface lowering (soil denudation) and related soil erosion rates over varying and long time intervals (virtually continuous and over millennia). To understand the dynamics of surface lowering and related soil erosion, it would be helpful to compare past erosion rates with present-day rates. Actual (average) rates can be determined with nuclear fallout radionuclides (Lal, Tims, Fifield, Wasson, & Howe, 2013; Meusburger et al., 2016). Isotopes of plutonium ($^{239+240}\text{Pu}$) are an efficient tool in tracing soil erosion and accumulation (Alewell, Pitois, Meusburger, Ketterer, & Mabit, 2017).

This combined approach should enable us to compare past long-term soil denudation rates with the present-day soil erosion rates. This gives us a hint about the future surface development. We thus had the following research questions:

1. How did soil denudation and, thus, soil erosion rates vary over late Pleistocene-to-Holocene time?
2. How did soils develop over time? Can progressive and regressive phases be detected?
3. How do current soil erosion rates compare to past rates?

2 | STUDY AREA

The Sila Massif upland in Calabria, southern Italy, was chosen (Figure 1c), because of its ideal geomorphological and geological setting (Figure 1d). The tectonic massif started forming during the active subduction of the Ionian Basin along the Calabrian Arc (Figure 1e) in the Oligocene (Rossetti et al., 2001). Several tectonic phases uplifted the Sila Massif mainly during the Miocene to the late Pleistocene (Olivetti, Cyr, Molin, Faccenna, & Granger, 2012). The relief and drainage systems are nowadays controlled by N-S, E-W, and NW-SE trending faults (Molin, Pazzaglia, & Dramis, 2004; Spina, Galli, Tondi, Critelli, & Cello, 2007).

The solitary position and surrounding steep slopes (Figure 1c) make the plateau an independent rock mass system. The old landscape of the Sila upland has been affected by long-term deep weathering processes (Figure 2) and subsequent erosion (Scarciglia, 2015; Scarciglia et al., 2016). As a consequence of weathering, granitic boulder fields, tors, and bornhardt landforms have developed here (Scarciglia, 2015). The present-day landscape has many tor and bornhardt landforms and is generally characterised by wide, gently rolling to flat palaeosurfaces ranging from 1,000 to 1,700 m asl. They represent remnants of old planation landforms that were shaped since the Pliocene to the Pleistocene (Molin et al., 2004; Sorriso-Valvo, 1993).

Soils are predominately Cambisols and Umbrisols and occasionally Leptosols, Fluvisols, Regosols, and Andosols (Scarciglia, Le Pera, & Critelli, 2005a). The soils are affected by volcanic ash input, which derives mostly from the Lipari Islands, and started to form during the Pleistocene (Raab et al., 2017). The overall soil thickness can reach 80–100 cm whereby the upper A, A1, or Ap horizons are about 10–35 cm thick (Table 1). Bt and Bw horizons are found in 30- to 60-cm depth. Above the C horizon, in about 60–75 cm, a Bw2 and

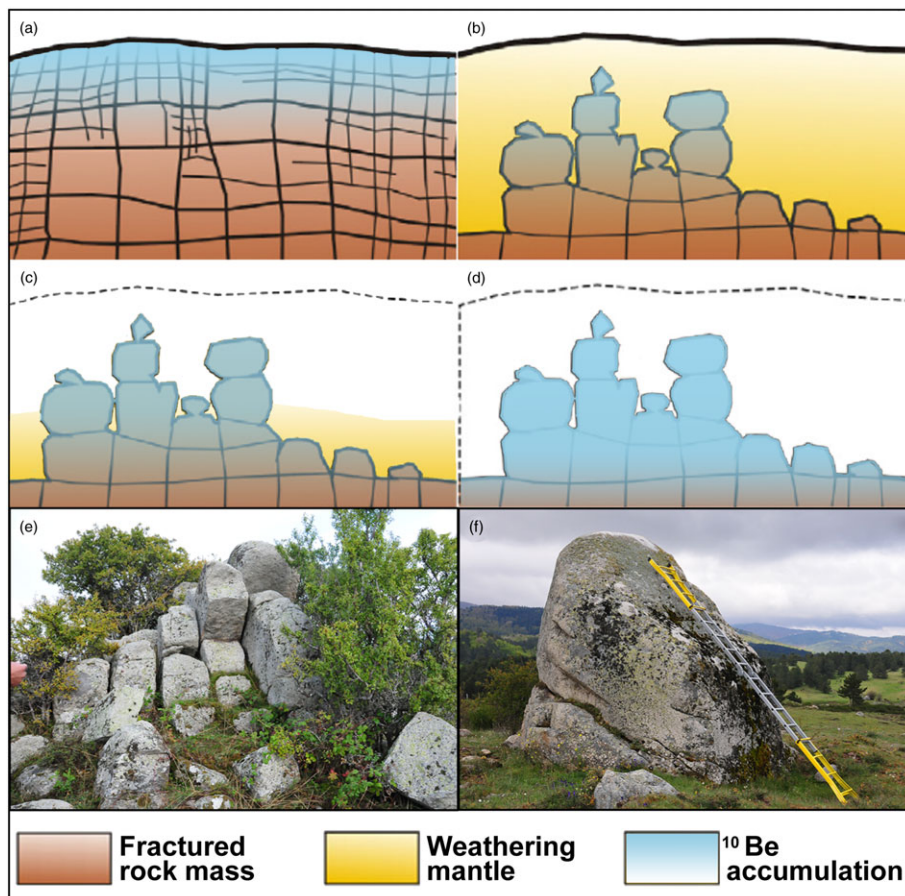


FIGURE 2 Weathering scheme of a rock surface (Migoñ, 2013). It starts with (a) rock fracturing, followed by (b) the formation of a deep weathering mantle and (c) erosion of the weathering mantle over time until (d) present-day surface has established. The bluish colour indicates the hypothesised increasing accumulation of ^{10}Be over time. (e,f) A local example of this process [Colour figure can be viewed at wileyonlinelibrary.com]

CB (t) is quite common (Scarciglia, Le Pera, Vecchio, & Critelli, 2005b; Raab et al., 2017).

The vegetation cover of the Sila upland plateau consists of grassland, conifers (pines and firs), and deciduous trees (beech; Scarciglia, Le Pera, & Critelli, 2005a; Sorriso-Valvo, 1993). The present-day temperate climate is typical for upland Mediterranean zones having an annual average temperature of 9–12°C and an annual precipitation of 1,000–1,800 mm (Le Pera & Sorriso-Valvo, 2000).

3 | MATERIALS AND METHODS

3.1 | General procedure

A multimethodological approach was chosen to address our research questions. We used the following methods to obtain soil denudation (erosion) rates for the Sila plateau:

- Vertical sampling of tors and determination of the speed of their long-term exhumation rate to derive soil denudation rates using in situ ^{10}Be .
- Sampling of soils near the tors. This was done with the purpose to obtain quantitative current (last 50 years) and indicative mid-

term (decade/century) soil erosion rates by using the fallout radionuclides $^{239+240}\text{Pu}$ and stable carbon isotopes ($\delta^{13}\text{C}$).

In addition, larger scale catchment-wide erosion values (based on ^{10}Be measurements on fluvial sediments) are available for this area and are used for comparison (Olivetti et al., 2012).

3.2 | Sampling of tors for in situ ^{10}Be dating and long-term soil denudation

We sampled three tors having a height of some metres (Figure 3, Table S1). The sampling was carried out (Figure 3b,c) at different heights on the tors in order to assess their possibly multistep exhumation through time. In total, we took six 1- to 3-kg samples of rock per tor at increasing heights from the base, using an electrical stone saw, hammer, and chisel. We sampled the uppermost 1–3 cm of the rock surface and documented the sample thickness (Table S1).

Principally, the longer the surface is exposed to cosmic rays, the more in situ ^{10}Be is accumulated. Due to the fact that ^{10}Be also penetrates the soil surface and that consequently some tors may already have interacted with cosmic rays before they appear at the surface, we also sampled tors below the surface (up to 40 cm) to account for

TABLE 1 Soil features of the Sila Massif upland

Label	Horizon	Depth (cm)	Munsell colour (moist)	Structure	Texture	Organic matter (%)	pH (-)	Sand (%)	Silt (%)	Clay (%)
Scarciglia, Le Pera, Vecchio, and Critelli (2005b):							(H ₂ O)			
P1	A1	0–5/10	10YR 2/2	m, C, m SB	SL	9.3	5.4	56.4	35.6	8.0
	A2	5/10–55	10YR 2/2	m/c AB	L	3.1	5.8	44.6	45.4	10.0
	Bw	55–75	10YR 4/4	m SB	SL	1.0	6.0	59.4	30.6	10.0
	C	75–110+			SG					
P2	A	0–10	10YR 4/2	m SB, vc C	LS					
	Bw1 + Bw2 + Bw3	10–125	10YR 5/4–4/4	m/c SB	LS	0.6	6.1	75.4	16.6	8.0
	Bw4	125–158	10YR 4/2	c SB	LS	1.1	6.1	68.4	19.6	12.0
	2Ab	158–190	10YR 2/2	c AB	SL	3.2	6.2	55.8	32.2	12.0
	2Bwb	190–230	10YR 6/6	m SB	LS	0.5	6.5	75.4	18.2	6.0
	2BC	230–260+	10YR 6/6	m SB	LS					
P3	Oi	0–5								
	A1	5–20/30	10YR 2/2	C C, m SB	L	5.7	5.7	54.6	37.4	8.0
	A2	20/30–45	10YR 2/2	c AB	L	5.4	6.1	46.0	45.0	9.0
	A3	45–60/65	10YR 3/2	f SB	L	3.7	5.9	46.8	45.2	8.0
	2Bw1	60/65–80	7.5YR 4/3	c SB	L	0.9	6.4	57.0	35.0	8.0
	2Bw2	80–100	7.5YR 4/4	c SB	SL	0.6	6.2	61.8	28.2	10.0
	2BC	100–120+	7.5YR 5/4	m SB	SL					
P4	Oi	0–2								
	A	2–25	10YR 3/3	c C, m AB	LS	3.6	5.8	80.6	17.4	2.0
	R	25–60+								
P5	A	0–30/38	10YR 4/4	m C, m SB	L	3.1	5.0	42.6	43.8	13.6
	Bt	30/38–60	7.5YR 4/6	c AB	L	0.9	5.5	37.8	36.6	25.6
	CBt	60–75	7.5YR 4/3	m SB	SL	0.4	5.6	74.4	10.0	15.6
	C	75–100+			S					
Raab et al. (2017):							(CaCl ₂)			
Sila I	A1	0–20	10YR 3/4			10.1	4.8	37.1	38.0	24.9
	A2	20–40	10YR 3/4			6.7	5.0	-	-	-
	Bw	40–60	10YR 4/6			1.3	5.0	60.7	33.4	5.9
	2Bw	60–80	10YR 6/4			1.4	5.1	-	-	-
	2C	80–100	10YR 6/3			0.7	4.9	70.9	22.4	6.7
Sila II	A1	0–20	10YR 3/4			9.0	5.1	-	-	-
	A2	20–40	10YR 3/4			6.1	5.0	-	-	-
	Bw	40–60	10YR 4/6			3.3	5.1	-	-	-
	2Bw	60–80	10YR 6/4			0.9	5.2	-	-	-
	2C	80–100	10YR 6/3			0.9	5.2	-	-	-

Note. The profiles P1–P5 are south of Cecita Lake (near Location 2) and Sila I and II are at Location 1 (Figure 3). Structure: AB: angular blocky; SB: subangular blocky; C: crumbly; f: fine; m: medium; c: coarse; vc: very coarse. Texture: L: loam; SL: sandy loam; LS: loamy sand; S: sand; SG: sandy gravel.

this early subsurface ¹⁰Be accumulation (Figure 3d). The GPS position of each of the sampling sites was recorded and verified with topographic maps. Both the geometry of each tor and the topographic shielding by the surrounding terrain influence the amount of cosmic radiation received at each location. We corrected for these effects, by measuring the dip of the rock surface, its direction, and topographic shielding.

3.3 | Laboratory procedure for surface exposure dating (¹⁰Be)

The sampled rock material was crushed and the 0.6- to 0.25-mm fraction collected (Kohl & Nishiizumi, 1992). The material was then treated

using standard procedures: aqua regia for 36 hr to eliminate iron oxides, carbonates, and organic material; 1 hr treatment with 0.4% hydrogen fluoride (HF) and a floatation system (Kitchener, 1984) to physically separate feldspar and mica components from quartz; and final leaching with 4% HF (7–21 days). A ⁹Be carrier solution (Scharlau, BE03460100) was added to 20–30 g of pure quartz and dissolved in 40% HF. Be was isolated using anion and cation exchange columns (von Blanckenburg, Belshaw, & O'Nions, 1996), and the obtained Be (OH)₂ was calcinated for 2 hr at 850°C to BeO and mixed with Nb powder (and transferred to targets). The targets were measured at the ETH Laboratory of Ion Beam Physics Accelerator Mass Spectrometry facility using the ¹⁰Be standard S2007N with a nominal value of ¹⁰Be/⁹Be = 28.1 × 10⁻¹² (Christl et al., 2013; Kubik & Christl, 2010).

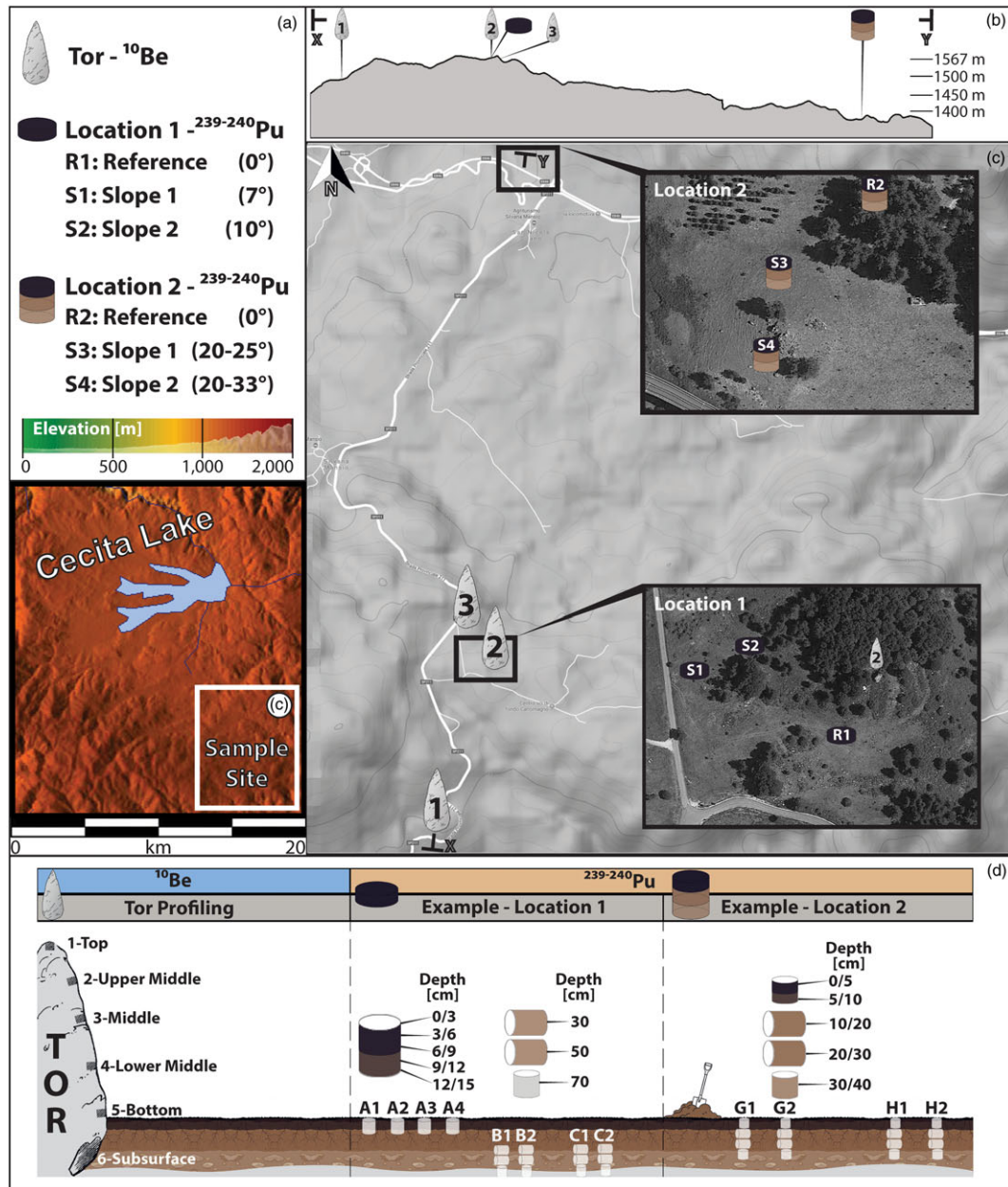


FIGURE 3 (a) Legend for the map symbols and sampling site within the study area. (b) X and Y mark the start and end points of the elevation profile (Google Earth, 2017). (c) Position of the sampled tors (Google Maps, 2017), with close-ups of the soil pits of Locations 1 and 2 (Google Earth, 2017). (d) Illustration of the individual sampling procedure in the field for ^{10}Be (five samples per tor) and $^{239+240}\text{Pu}$ (with four replicates for each sampling site) [Colour figure can be viewed at wileyonlinelibrary.com]

S2007N has been calibrated to the Nishiizumi standard ICN01-5-1 with a revised nominal value of 2.709×10^{-11} (Nishiizumi et al., 2007). The 1σ error of S2007N is 2.7% (Christl et al., 2013). Measured $^{10}\text{Be}/^9\text{Be}$ ratios were corrected for ^{10}Be contributed by the Be carrier (blank value: $3 \pm 0.87 \text{ E-15}$).

^{10}Be exposure ages were calculated using the cosmogenic nuclide online calculator v2.3 (Balco et al., 2008) with a sea-level high-latitude ^{10}Be production rate of 4.01 (^{10}Be atoms gram SiO_2^{-1} year $^{-1}$; Borchers et al., 2016), a ^{10}Be half-life of $1.387 \pm 0.012 \text{ Ma}$ (Chmeleff, von Blanckenburg, Kossert, & Jakob, 2010; Korschinek, Bergmaier, Faestermann, Gerstmann, & Remmert, 2010), a production rate correction for latitude and altitude (Lal, 1991; Stone, 2000), and a correction for sample thickness (Brown, Edmond, Raisbeck, Yiou, &

Desgarceaux, 1992) using an effective radiation attenuation length of 160 g cm^{-2} (Gosse & Phillips, 2001) and a rock density of 2.7 g cm^{-3} . We tested for various rock erosion rates (0, 1, and 2 mm kyr^{-1}) to cover a greater range of potential variability and, thus, ages and applied no correction for snow.

3.4 | Determination of surface lowering and soil denudation/erosion rates using ^{10}Be

Ages calculated assuming a rock erosion rate of $0-1 \text{ mm kyr}^{-1}$ were used for model fitting (height vs. age). Best regression fits were obtained with a polynomial (third order) and a logistic model (Lichter, 1998),

$$f(t) = \frac{a}{(1 + e^{b(t-c)})} + d, \quad (4)$$

where $f(t)$ is the height (m; lowered surface), as a function of time, a the range of height (m), t the time (year), b the slope coefficient (-), c the time of the maximal rate of change (year), and d the asymptotic value (m). By taking the error ranges of the ^{10}Be measurements into account (external error), we modelled the height–age relation using Monte Carlo simulations and the previously noted regression fits.

The mathematical derivation of these functions then provided rates in form of surface lowering (SL) (mm year^{-1}) and, thus, the amount of soil denudation over each time interval. To do this, the age of the rock's initial appearance at the surface (early subsurface ^{10}Be accumulation; t_s) had to be taken into account.

$$\frac{\partial f(t-t_s)}{\partial t} = SL(t). \quad (5)$$

The soil denudation rates ($t \text{ km}^{-2} \text{ year}^{-1}$), which are mostly due to soil erosion (see Equation (3)), were then obtained by

$$D_{\text{soil}} = E_{\text{soil}} = SL(t) \times \rho_s \times 1,000, \quad (6)$$

with ρ_s as the soil bulk density of 0.82 t m^{-3} .

3.5 | Short- and mid-term soil erosion

We used $^{239+240}\text{Pu}$ for the assessment of the current (last few decades) soil redistribution rates. Because they were emitted during the nuclear weapon tests of the mid-20th century (maximum in 1963–1964), Pu isotopes provide an average soil redistribution rate for the last ~50 years (Wallbrink & Murray, 1993). Soil redistribution rates are calculated on the basis of the differences in Pu activity (Bq m^{-2}) between a local flat reference site and inclined investigation sites (e.g., eroding slopes). It is expected that the 'erosion' sites have a lower Pu activity than the 'reference' site. The signature of stable carbon isotopes and total soil organic carbon content allowed us to qualitatively indicate mid-term disturbances in soils (Zollinger et al., 2015). Due to fractionation during organic matter decomposition, an enrichment of ^{13}C together with a decrease in the C content with increasing soil depth is expected (Schaub & Alewell, 2009).

We choose undisturbed reference soil locations with a flat topography and slopes of varying angles in close proximity as erosion/accumulation sites. We sampled four replicate soils at each of the reference (R) and erosion sites (S1–S4; Figure 3d). In total, three sampling series at two locations were undertaken, whereby Location 1 is associated with Tor 2 for better comparability (Figure 3c). Samples were collected using a 5-cm-diameter core sampler. Soil cores were taken at 3- to 5-cm increments from 0- to 20-cm depths and at higher increments below 20-cm depth (to a maximum depth of 70 cm at Location 1 and to 40 cm at Location 2) at all erosion and reference sites. The soil cores were also used to determine soil bulk densities. A total of 156 soil samples were analysed for Pu and C isotopes.

3.6 | Determination of $^{239+240}\text{Pu}$ in soil samples

The measurement of Plutonium isotopes ($^{239+240}\text{Pu}$) was performed at Northern Arizona University using a Thermo X Series II quadrupole inductively coupled plasma mass spectrometry (ICP-MS) instrument equipped with a high-efficiency desolvating sample introduction system (APEX HF, ESI Scientific, Omaha, NE, USA). A detection limit of $0.1\text{-Bq kg}^{-1} \text{ }^{239+240}\text{Pu}$ was obtained for samples of ~1 g of dry-ashed material (16 hr, 550°C). The measurement error was 1% to 3% for $^{239+240}\text{Pu}$ activities $>1 \text{ Bq kg}^{-1}$. Prior to ICP-MS analysis, the samples were dry ashed and spiked with ~0.005 Bq of a ^{242}Pu tracer (licensed solution from NIST). Pu was leached with 16-mol L^{-1} nitric acid overnight at 80°C and was subsequently separated from the solution using a Pu-selective TEVA resin (Ketterer, Zhang, & Yamada, 2011). The masses 235, 238, 239, 240, and 242 were recorded. Taking the mass bias factor and the UH^+/H^+ ratio into account, the individual mass ratios were corrected and the $^{240}\text{Pu}/^{239}\text{Pu}$ atom ratios determined. Data quality was evaluated through the analysis of blanks (soils or rocks devoid of Pu), duplicates, and control samples having known $^{239+240}\text{Pu}$ activities.

3.7 | $^{239+240}\text{Pu}$ activity conversion into soil redistribution rates

As a basis for the calculation of soil accumulation or erosion rates, the inventory (I) of the $^{239+240}\text{Pu}$ activities (Bq m^{-2}) has to be determined by using the equation

$$I = \frac{1}{A} \sum_i M_i C_i, \quad (7)$$

where A is the horizontal cross-sectional area (m^2), M_i the mass (kg) of the i th sample depth increment, and C_i the activity (Bq kg^{-1}) of the i th subsample depth increment.

Soil redistribution rates were then obtained when the isotope inventory for an eroding point was compared with a local reference inventory where neither soil erosion nor soil accumulation is expected. Two different models were used to convert $^{239+240}\text{Pu}$ inventories into soil redistribution rates:

1. The profile distribution model after Walling and He (1999) and Zhang, Higgitt, and Walling (1990):

$$I'(x) = I_{\text{ref}} \left(1 - e^{-\frac{M_x}{h_0}} \right), \quad (8)$$

where $I'(x)$ is the amount of the isotope inventory (Bq m^{-2}) above the depth (x), I_{ref} the reference inventory (Bq m^{-2} ; Location 1), M_x the mass (kg m^{-2}) between top and actual depth (x), and h_0 the profile shape factor (kg m^{-2}). The soil erosion rate E_{soil} ($\text{t km}^{-2} \text{ year}^{-1}$) was calculated using

$$E_{\text{soil}} = \frac{10}{t-t_0} \times \ln \left(\frac{1 - \frac{I_{\text{ref}} - I_{\text{inv}}}{I_{\text{ref}}}}{1 - \frac{I_{\text{ref}} - I_{\text{inv}}}{I_{\text{ref}}}} \right) \times h_0 \times 100, \quad (9)$$

where t is the year of sampling (2015 and 2016), $t_0 = 1,963$ (maximum peak of thermonuclear weapon testing), and I_{inv} is the investigation site inventory (Bq m^{-2}).

2. The inventory method according to Lal et al. (2013) calculating the loss of soil, L (Bq m^{-2}):

$$L = \frac{1}{\alpha P} \times \ln \left(1 - \frac{I_{\text{ref}} - I_{\text{inv}}}{I_{\text{ref}}} \right) \quad (10)$$

where α is the coefficient of the least squares exponential fit of the profile depth to activity after Alewell, Meusburger, Juretzko, and Mabit (2014) and P is the particle size correction factor. For both models, a p value of 1, 1.2 (Walling & He, 1999), and 1.5 (Lal et al., 2013) was used.

3.8 | Soil sample preparation, organic C, and stable carbon isotopes

Soil samples were oven dried at 70°C for 48 hr before being sieved to <2 mm (fine earth). Soil density was obtained from the dry weight of the 100-cm³ soil cores. Oven-dried fine earth samples were then fine milled. The organic carbon (C_{org}) contents were obtained by measuring 0.1-g finely milled soil material in tin capsules with a Leco® C-H-N elemental analyser (Leco TruSpec Micro Analyser) at the Zurich University of Applied Sciences. The EDTA standard (CAS No: 20824-56-0) and the Soil-Leco (Part No: 502-308) were used for standardisation.

The $\delta^{13}\text{C}$ isotopic ratios were measured with a Picarro analyser for isotopic CO_2 (Combustion Module Cavity Ring-Down Spectroscopy, Sunnyvale, California, USA). Instrumental precision is <0.1‰. Soil powder (milled fine earth) was weighed (~0.1 g) into tin capsules and combusted at 950°C. The released CO_2 was measured with a Cavity Ring-Down Spectroscopy analyser (G2131-i). We used an internal standard (30B00GW9 Chernozem 2013) for every six samples to correct for potential drift (<0.5‰) in the C and $\delta^{13}\text{C}$ values.

4 | RESULTS AND DISCUSSION

4.1 | Ancient surface denudation and long-term soil redistribution— ^{10}Be

The 18 collected rock samples (Table S1) provided 15 exposure ages ranging from 10 ± 2 to 106 ± 12 ka (Table S2). The applied different rock erosion rates (0, 1, and 2 mm kyr⁻¹) exerted only a minor influence (average 2.6 ka) on the calculated exposure ages (Figure 4). With a rock erosion of 1 mm kyr⁻¹, Tor 1 has an age of 37 ± 4 ka at 4 m above ground and Tor 3 an age of 36 ± 3 ka at 3.5 m above ground. Tor 2 yielded older overall ages (~100 ka) than Tor 1 and Tor 3, due to its greater height with 5.6 m. The vertical profile sampling series of each tor showed an increasing age trend (Figure 4a,c,e) along with higher ^{10}Be concentrations (Figure 4g) towards the tors' top surfaces. The increase in the ^{10}Be concentration with tor height reflects the conceptual idea that tors are exhumed over time at our study area. The tor assemblage shows consistent exhumation trends. The average exhumation rates were 0.054 ± 0.027 , 0.052 ± 0.026 , and 0.050 ± 0.026 mm year⁻¹, respectively. Obstacles that could have led to abrupt changes of the ^{10}Be signal (e.g., exfoliation) were not observed in field. Samples taken to determine early subsurface ^{10}Be accumulation had similar atom counts as the bottom-most tor surface

samples. Based on these indifferent results, we can assume that the surface lowering has occurred in a similar manner across the plateau. The calculated exhumation rates, therefore, represent a net soil denudation that is almost equal to soil erosion (Equations (3) and (6)).

Soil denudation/erosion rates over time were modelled by using the surface ages (and, thus, the tors' exhumation rates; Figure 4b,d,f). The rates are in the range of 50–300 t km⁻² year⁻¹ for the last 25 ka (Figure 4b,f). Due to the greater size of Tor 2 and, thus, older ages (Figure 4c), its model provides insight over the last 100 ka and indicates rates of 0–130 t km⁻² year⁻¹ (Figure 4d). By combining the information derived from all tors, we constructed a relatively detailed time sequence for the last ~100 ka (Figure 4h).

The total soil denudation rates have clearly changed over time. The lowest rates were calculated for the period 100–20 ka BP. Higher rates are seen before 100 ka BP and after 20 ka BP. Soil erosion rates showed a maximum of about 250 t m⁻² year⁻¹ (about 0.31-mm year⁻¹ soil material) at the transition from the Pleistocene to the Holocene. Minimum rates were measured around 50–100 ka BP with about 0–0.12 mm year⁻¹. Based on earlier geomorphological and pedological investigations, Scarciglia (2015) and Scarciglia et al. (2016) estimated the average erosion rates for the Sila upland to be in the range of <0.01–0.05 to 0.10–0.21 mm year⁻¹. With a soil density of approximately 0.82 g cm⁻³, the soil erosion rates vary between 8 and 170 t km⁻² year⁻¹. These values fit well with the rates that we obtained.

Our values are also consistent with uplift-driven Pleistocene–Holocene erosion rates (0.04–0.6 mm year⁻¹; about 30–490 t km⁻² year⁻¹), estimated for various areas of the southern Apennines (north of Calabria; Amato, Aucelli, & Cinque, 2003; Gioia, Martino, & Schiattarella, 2011; Martino, Nico, & Schiattarella, 2009). Catchment-wide average erosion rates of the steep slopes at the border of the Sila upland are given in Olivetti et al. (2012). These rates vary between 0.08 and 0.92 mm year⁻¹ (expressed on the basis of quartz with a density of 2.6 g cm⁻³) or about 216–2,480 t km⁻² year⁻¹. Catchment-based erosion rates, however, include all erosion processes, not all of which are related to soil.

4.2 | Qualitative soil erosion estimates— $\delta^{13}\text{C}$

The $\delta^{13}\text{C}$ values of all soil sites (Table S3) increase with soil depth and range between –28‰ and –25‰ (Figure 5). In contrast, total C_{org} decreases with depth. Therefore, all investigated soil profiles exhibit a negative linear correlation between $\delta^{13}\text{C}$ and C_{org} . The negative correlation of C_{org} and $\delta^{13}\text{C}$ can qualitatively indicate the extent of mid-term disturbances in soils (Zollinger et al., 2015). However, when only erosion (and no accumulation or mixing) occurs, the depth trends of C_{org} and $\delta^{13}\text{C}$ still remain similar. The lowest correlations ($\rho = -0.87$) are calculated for flat surfaces (0°) of the R sites and slightly higher correlations ($\rho = -0.89$ to -0.93) for slopes. We also obtained a C_{org} content of <0.5% at 40–70 cm, whereas the $\delta^{13}\text{C}$ values showed a large variability (most likely due to increasing accuracy problems with a low carbon content). These $\delta^{13}\text{C}$ values were not considered for the correlation calculations. In contrast to findings of Zollinger et al. (2015), our $\delta^{13}\text{C}$ trends did not indicate any particular disturbances that could be directly related to erosion/accumulation.

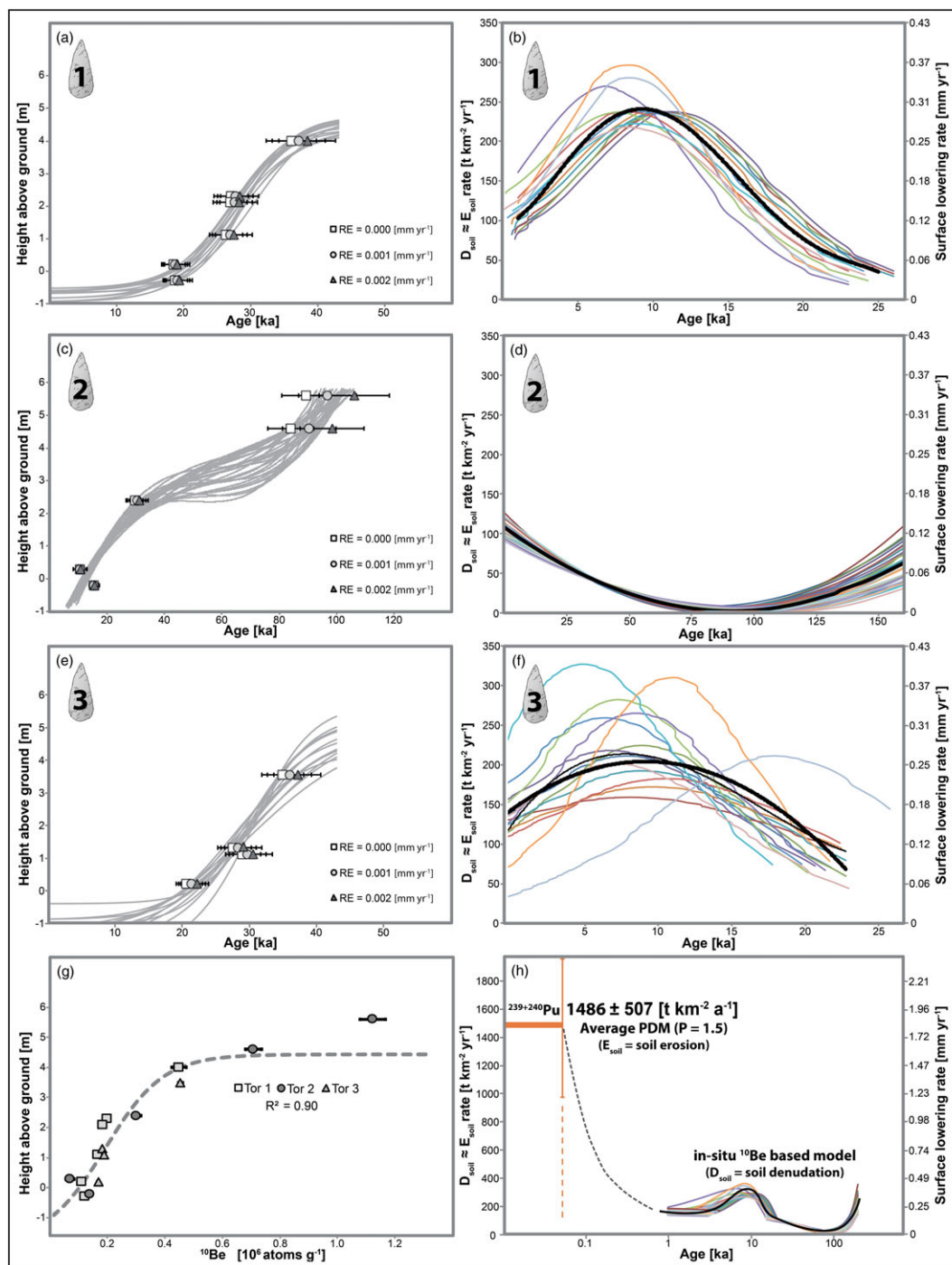


FIGURE 4 Exposure ages (^{10}Be) as a function of tor height and derived soil denudation/erosion rates (using a Monte Carlo simulation) for Tor 1 (a,b), Tor 2 (c,d), and Tor 3 (e,f). ^{10}Be concentrations as a function of height (with a related trend curve) of all samples are plotted in (g). Temporal evolution of soil denudation/erosion rates (h) using both, ^{10}Be and $^{239+240}\text{Pu}$ data. For simplicity, soil erosion is assumed to be almost equal to soil denudation (see Equations (2), (3), and (6)) [Colour figure can be viewed at wileyonlinelibrary.com]

4.3 | Modern soil erosion rates of the Sila upland— $^{239+240}\text{Pu}$

The $^{240}\text{Pu}/^{239}\text{Pu}$ atomic ratios of all samples (Figure 6a) lie within the characteristic signature of the fallout in the northern hemisphere (0.180 ± 0.014 ; Kelly et al., 1999) and do not indicate contributions or influences from any regional source(s). Reference and

erosion sites have a similar and consistent $^{240}\text{Pu}/^{239}\text{Pu}$ signals throughout all depth increments. Only a few samples of Location 1 have slightly higher values (up to 0.248 ± 0.0045).

The $^{239+240}\text{Pu}$ activity distributions (Figure 6b) along the profiles of Location 2 are consistent with observed trends in the literature, where higher activities were reported to occur near the surface and exponentially decrease with depth (Alewell et al.,

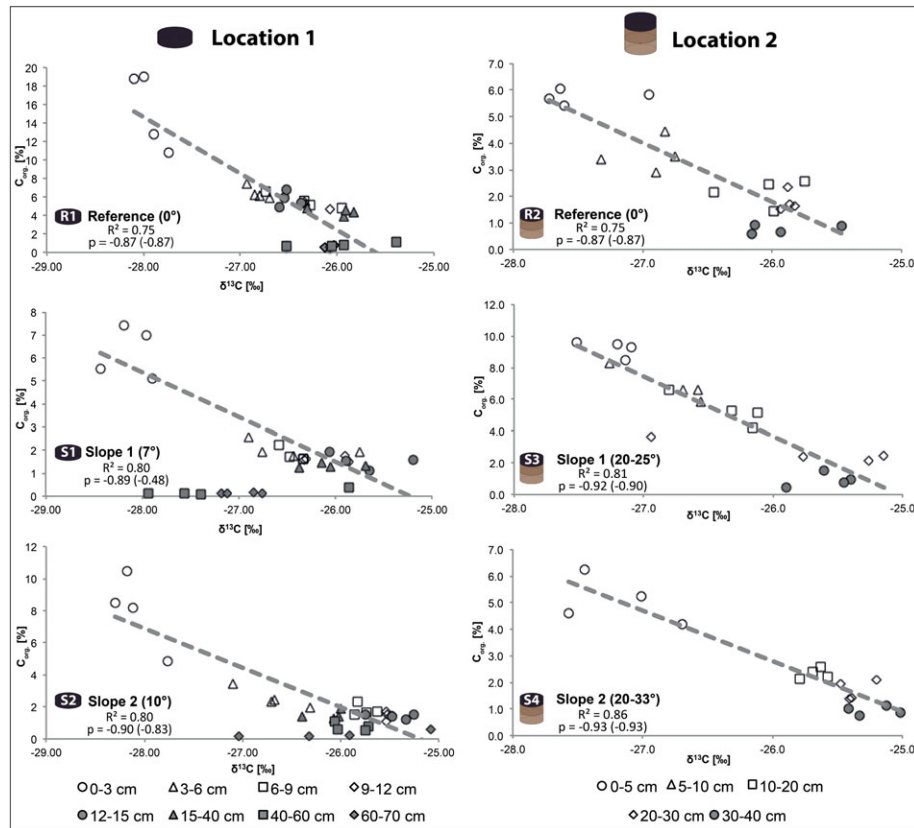


FIGURE 5 Correlation between C_{org} (organic carbon content) and $\delta^{13}C$ values as indicator of soil disturbance/stability. Below a concentration of 0.5% of C_{org} , $\delta^{13}C$ could not be measured accurately enough; these values were not considered for the correlation [Colour figure can be viewed at wileyonlinelibrary.com]

2014; Portes et al., 2018; Lal et al., 2013, Meusburger et al., 2016; Zollinger et al., 2015). In contrast, Location 1 has an unusual Pu depth trend, although similar activity trends were reported by Ketterer et al. (2004) and Frielinghaus and Vahrson (1998). At Location 1, bioturbation (visible in the field) seems to have been one cause for the unusual Pu depth trend. The $\delta^{13}C$ data however indicate (Figure 5) that not only bioturbation but also other processes such as a translocation with colloids (clays) may have contributed. The pH values of the soils (Table 1) are in the appropriate range to indicate that clay migration is reasonable. To a limited extent, Pu is also involved in soil-forming processes (Bunzel, Kracke, & Schimmak, 1995).

Nevertheless, the Pu total inventory (Figure 6b) reflects the expected erosional behaviour signal of the study sites, where a lower activity was measured on slopes than on flat surfaces. The highest total inventory of $176 \pm 18 \text{ Bq m}^{-2}$ was determined for R1. This quantity was used as basis for the profile distribution model and inventory method. Our $^{239+240}\text{Pu}$ data indicate soil erosion at all investigated sites (Figure 6c, Table 2). Interestingly, the $^{239+240}\text{Pu}$ activity ($\sim 0.8 \text{ Bq kg}^{-1}$) at Location 2 in the topsoil is quite similar to the site R1 at 15-cm depth ($\sim 0.7 \text{ Bq kg}^{-1}$; Figure 6b). We assume that the soil at Location 2 has lost part of its uppermost layer (first $\sim 15 \text{ cm}$) in the recent past. Observations of erosion rims (sometimes $>30 \text{ cm}$; with traces of clay coatings on the rock) between the present-day soil surface and boulders or tors also indicate recent erosion events (Scarciglia, 2015).

Furthermore, the soil erosion rates (Figure 6c) of Location 2 are distinctly higher than those of Location 1. The erosion rates at Site 1 vary from $1,000$ to $2,100 \text{ t km}^{-2} \text{ year}^{-1}$ whereas erosion rates range from $1,200$ to over $3,500 \text{ t km}^{-2} \text{ year}^{-1}$ at Site 2. Soil erosion rates are also found to be higher along steeper hill slopes (Figure 6d). The fact that soils of Location 2 have steeper slopes and are shallower compared with Location 1 further supports our assumption that Location 2 has recently lost part of its uppermost layer.

In general, the recent soil erosion rates in the Sila upland (on slopes) with about $1,000$ to more than $3,000 \text{ t km}^{-2} \text{ year}^{-1}$ are very high. According to Alewell, Egli, and Meusburger (2015), soil erosion rates in alpine areas at intensively used slopes ranged from 600 to $3,000 \text{ t km}^{-2} \text{ year}^{-1}$. Such rates are certainly not compatible with a sustainable use of soils.

4.4 | Past progressive and regressive soil formation

To estimate tolerable rates of soil erosion/denudation, it is important to know the soil production/formation rates that are counteracting soil loss processes (Alewell et al., 2015; McFadden, 2013). Several empirical investigations show that the rate of soil production or soil formation is a function of time (e.g., Alewell et al., 2015; Anderson, Dietrich, & Brimhall, 2002). According to Alewell et al., average soil production rates in alpine areas for relatively old soils ($>10\text{--}18 \text{ ka}$) range around $54\text{--}113 \text{ t km}^{-2} \text{ year}^{-1}$. Production rates for young soils ($>1\text{--}10 \text{ ka}$) are between 119 and $248 \text{ t km}^{-2} \text{ year}^{-1}$, and rates for very

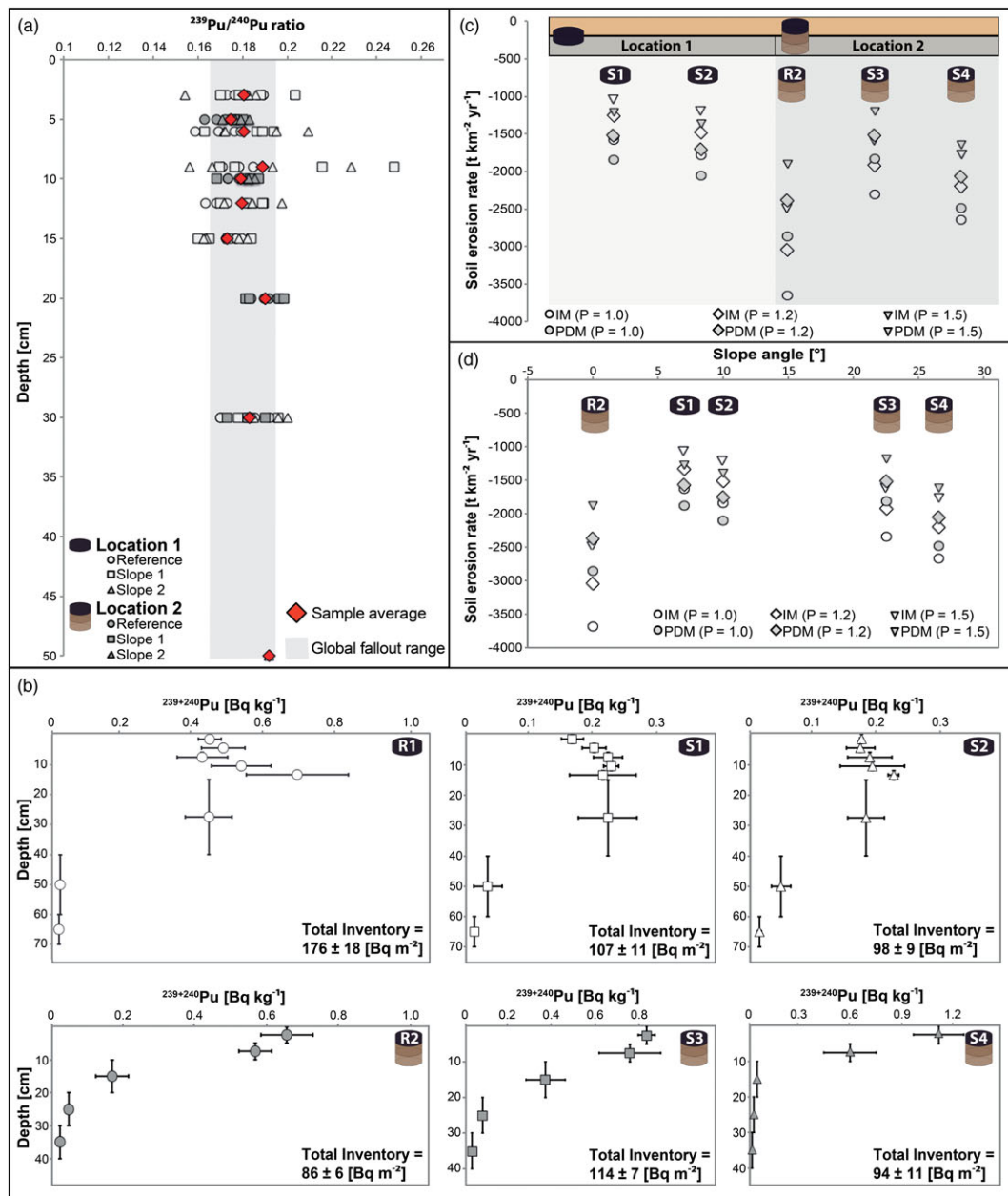


FIGURE 6 (a) $^{240}\text{Pu}/^{239}\text{Pu}$ ratio of the soil samples as a function of soil depth. The average for each depth increment is given in red. The grey area indicates the global fallout range (0.180 ± 0.014) of the northern hemisphere (Kelly, Bond, & Beasley, 1999). (b) Depth activity profiles (\pm standard error) of the investigated sites. (c) Calculated annual soil erosion using different particle size correction factors ($p = 1.0, 1.2,$ and 1.5) for the inventory method (IM; R Lal et al., 2013) and the profile distribution model (PDM; Walling & He, 1999; Zhang et al., 1990). (d) Calculated soil erosion ranges in relation to the slope angle [Colour figure can be viewed at wileyonlinelibrary.com]

young soils (≤ 1 ka) are between 415 and $881 \text{ t km}^{-2} \text{ year}^{-1}$. Dixon and von Blanckenburg (2012) estimated a maximum soil production rate in the range of $320\text{--}450 \text{ km}^{-2} \text{ year}^{-1}$, whereas Alewell et al. (2015) and Larsen et al. (2014) set this value much higher (for very young soils or highly eroding sites up to $2,000 \text{ t km}^{-2} \text{ year}^{-1}$). The average soil denudation rates for the Sila plateau over the last 20 ka are about $145 \text{ t km}^{-2} \text{ year}^{-1}$.

Overall, the soil denudation/erosion rates have strongly varied in the Sila mountains. At the transition from the Pleistocene to the Holocene, we observe rates of up to $300 \text{ t km}^{-2} \text{ year}^{-1}$. This fits well with findings of Zanchetta, Borghini, Fallick, Bonadonna, and Leone (2007) and Tinner et al. (2009) who showed that a

higher frequency of forest fires occurred at the onset of the Holocene. The presence of organised human societies since the Bronze Age in southern Italy and the Baleari Islands, around 4,000 cal BP, was detected by a repeated increase in fire events, which are most likely of anthropogenic origin (Peréz-Obiol & Sadori, 2007). Pollen analyses of the Lago Grande di Monticchio clearly show that the Apennine mountain chain was increasingly influenced by forest clearance and agricultural activity over the last 2,000 years (Allen, Watts, McGee, & Huntley, 2002)—a phenomenon that is also documented in the Sila upland by pedological, charcoal, and historical data (Moser, Di Pasquale, Scarciglia, & Nelle, 2017; Pelle et al., 2013; Scarciglia et al., 2008).

TABLE 2 Calculated soil erosion rates of $^{239+240}\text{Pu}$ investigated soil pits of Location 1 (S1 and S2) and Location 2 (S3, S4, and R2) after Lal et al. (2013), Walling and He (1999), and Zhang et al. (1990) applying diverse particle size correction factors (PM)

		Inventory method (IM)			Profile distribution model (PDM)		
		PM = 1 ($\text{t km}^{-2} \text{ year}^{-1}$)	PM = 1.2 ($\text{t km}^{-2} \text{ year}^{-1}$)	PM = 1.5 ($\text{t km}^{-2} \text{ year}^{-1}$)	PM = 1 ($\text{t km}^{-2} \text{ year}^{-1}$)	PM = 1.2 ($\text{t km}^{-2} \text{ year}^{-1}$)	PM = 1.5 ($\text{t km}^{-2} \text{ year}^{-1}$)
S1	Average	-1,585	-1,320	-1,056	-1,881	-1,568	-1,254
	Std. error	13.5	13.2	11.8	19.3	17.6	15.8
S2	Average	-1,813	-1,511	-1,209	-2,098	-1,748	-1,398
	Std. error	14.0	12.8	11.5	16.1	14.7	13.2
S3	Average	-2,307	-1,922	-1,538	-1,832	-1,527	-1,221
	Std. error	45.4	41.5	37.1	40.3	36.8	32.9
S4	Average	-2,640	-2,200	-1,760	-2,478	-2,065	-1,652
	Std. error	39.9	36.5	32.6	36.1	33.0	29.5
R2	Average	-3,649	-3,041	-2,433	-2,853	-2,378	-1,902
	Std. error	55.6	50.7	45.4	47.9	43.8	39.1
Total Average		-2,399	-1,999	-1,599	-2,228	-1,857	-1,486
Std. error		46	42	38	38	35	31

Note. Figure 6 provides a more graphical display.

Our compiled soil formation and soil production rates (Figure 7a,b) of Mediterranean to alpine climates demonstrate that several regressive soil evolutionary phases must have occurred at the investigated site. Only young soils (>1–10 ka) with high soil production rates would have been able to cope with the relatively high soil erosion rates ($\sim 300 \text{ t km}^{-2} \text{ year}^{-1}$) at the Pleistocene–Holocene transition. Only very young (≤ 1 ka) and shallow soils (~ 20 cm) have such high soil production rates that would equal the observed soil erosion rates for the last 50 years ($\geq 1,000 \text{ t km}^{-2} \text{ year}^{-1}$).

Based on our dataset, we estimated (very roughly) the counterpart of soil denudation over time (Figure 7c). The study area received ash input from volcanic eruptions on the Lipari Islands (Raab et al., 2017) several times (with three major eruptions) during the last 15 to 90 ka (that corresponds approximately to the duration of soil formation). Soil aggradation by ashes is also supported by field evidence (Scarciglia, 2015). The fresh and unweathered material serves as new substrate and counteracts soil erosion as explained in Ugolini and Dahlgren (2002). With each new ash input, the soil production rate increases drastically for roughly 800 years to a magnitude range of $\geq 1,000 \text{ t km}^{-2} \text{ year}^{-1}$ (Figure 7b,c). Due to the rejuvenation of the soil parent material, the soil production remained $>100 \text{ t km}^{-2} \text{ year}^{-1}$ for about 10 ka (Figure 7b,c). Although these estimates are only approximate, they nonetheless show that progressive phases of soil formation, presumably (vitric) Cambisols, occurred between about 55–30 ka BP and 20–15 ka BP (Figure 7c,d). The two dominating soil-forming processes were probably transformation through chemical weathering and addition of new material (volcanic glass and minerals) as well as decomposing (dead) plant tissue. We see that regressive phases prevail particularly during the last 15–20 ka where soil denudation rates increased to about $300 \text{ t km}^{-2} \text{ year}^{-1}$ and were, as an average, about 50–100 $\text{t km}^{-2} \text{ year}^{-1}$ higher than soil production rates (Figure 7c,d).

4.5 | Present situation and outlook

Although a large part of the Sila Massif is a forested national park, it is partly used for arable crops and livestock (sheep and cattle) and still records the effects of intensive land use of the recent past. Where intense grazing still exists or where arable farming still occurs, soil erosion rates are high. On flat surfaces and where human impacts are low (e.g., with forest cover), conditions close to steady state (Figure 7d) may be established between soil production and soil denudation (Scarciglia et al., 2016). The Pu data indicate soil erosion rates on slopes of $\geq 1,000 \text{ t km}^{-2} \text{ year}^{-1}$. These rates appear to be considerably higher than during the past 10–60 ka (Figure 7d).

Conforti et al. (2013) concluded that intensive land use and annual crops have greatly contributed to the sediment input of the nearby Crati basin (Figure 1c). Bajard et al. (2017) demonstrated that deforestation already in medieval times has led to erosion rates in mountain areas of the European Alps of $1,000 \text{ t km}^{-2} \text{ year}^{-1}$. Arable farming even caused erosion rates of up to $1,230 \text{ t km}^{-2} \text{ year}^{-1}$. Vanacker, Bellin, Molina, and Kubik (2014) stated that a decreasing vegetation cover leads to an exponential increase in total erosion rates. The results of Hewawasam, von Blanckenburg, Schaller, and Kubik (2003) suggest that soil is lost 10–100 times faster on agricultural land. It is therefore reasonable to assume that the episode of higher soil erosion rates (detected by the Pu isotopes) is caused by human impact (e.g., overgrazing, pasture, and deforestation).

Our understanding of the Sila upland is that soil erosion rates of about $200\text{--}300 \text{ t km}^{-2} \text{ year}^{-1}$ are the natural maximum. This natural maximum might be climate driven when looking at the timing of the increase in denudation/erosion (post-Last Glacial Maximum [LGM]; Figures 4h and 7d). The increase in denudation rates at the transition from a cold to a warm period (climate change) has also been reported by Schaller et al. (2016). The sea surface temperature of the

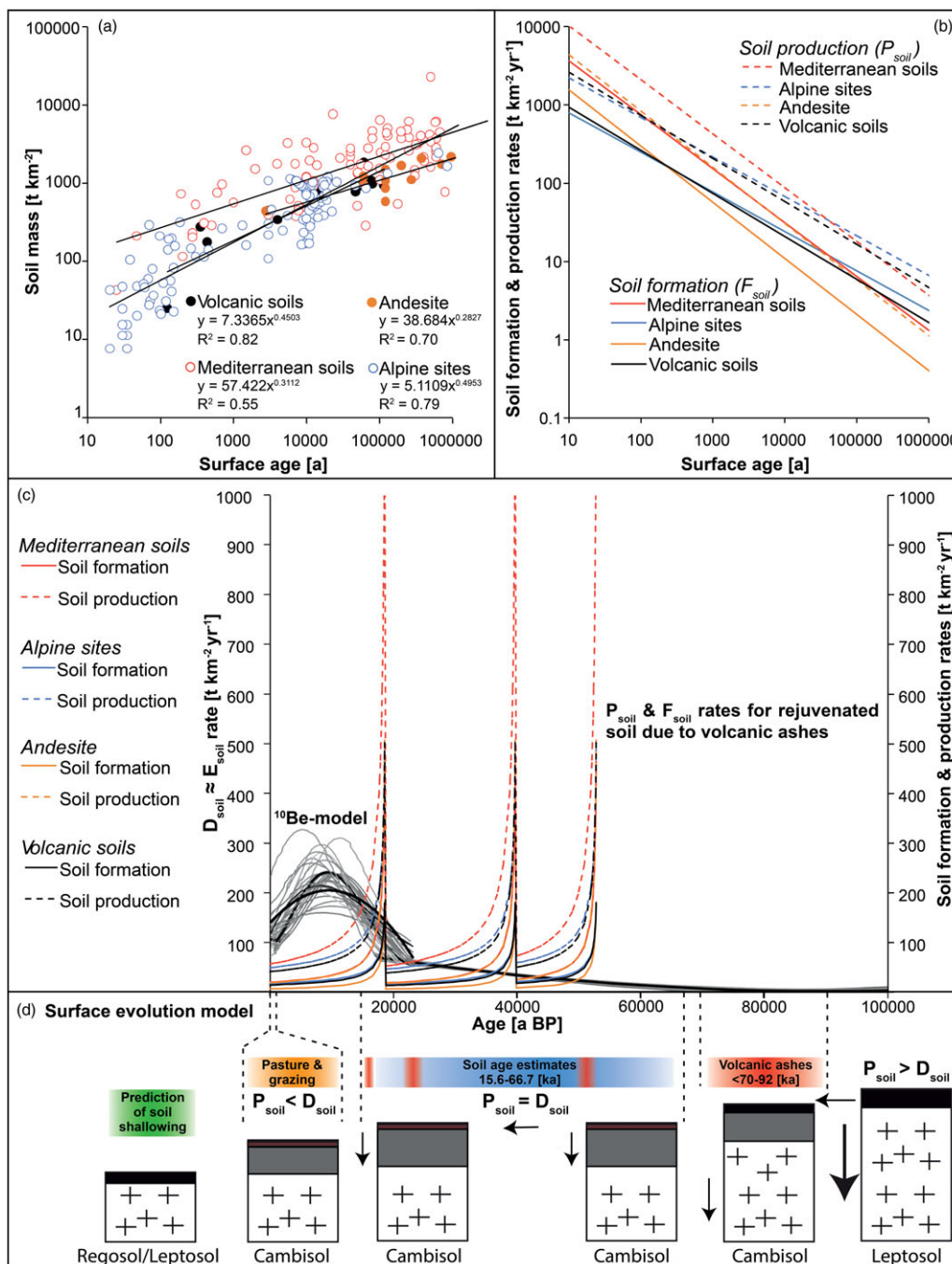


FIGURE 7 (a) Correlation between soil mass and surface age using chronosequences of volcanic, Mediterranean (and andesitic), and alpine soils after Egli et al. (2008, 2014, and references therein) and Alewell et al. (2015). (b) Mathematical derivation of the regression functions is given in (a). This derivation gives soil formation and production rates (Alewell et al., 2015) over time. (c) Comparison between soil denudation/erosion (black and grey lines; ¹⁰Be-based model) and soil formation/production rates (coloured lines) for the last 50 ka. Soil formation and production rates are derived from the regression curves given in Figure 7b. Over the entire soil formation period, three volcanic eruption periods (Lipari Islands) with subsequent ash input have occurred and led to a rejuvenation of the soils (Raab et al., 2017; Ugolini & Dahlgren, 2002). This gave rise to a sharp increase in the soil production and soil formation rate. (d) Conceptual model: Reconstruction of past and prediction of future soil evolution based on (c) and results from Raab et al. (2017) [Colour figure can be viewed at wileyonlinelibrary.com]

Tyrrhenian Sea (Figure 1c) started to rise ~18 ka BP; it reached its maxima around 8.9–8.4 ka BP (Cacho et al., 2001). This trend is similar to our denudation/erosion rates model (Figure 7c). Also, rapid environmental changes with increased moisture availability and biomass production in southern Italy (Lago Grande di Monticchio) were reported by Allen et al. (1999), starting ~15 ka ago. The abrupt warming and increase in precipitation after the LGM (Bølling transition) have

probably led to the increase in denudation/erosion up to its natural maximum around 9 ka ago.

The present-day use of the landscape often results in high erosion rates, which disrupts the balance between the natural removal of surface material and soil production. Steady-state conditions cannot be expected in such a situation. Therefore, the upland of the Sila Massif is now in a distinctly regressive phase with respect to soils. If the

current regressive phase of soil formation continues then Cambisols will—over long-time periods (century to millennia)—transform into a rockier landscape (Figure 7d) with very shallow Leptosols (soil depth < 5 cm) or Regosols (see Alewell et al., 2015).

5 | CONCLUSIONS

Our multi-isotope approach has allowed us to decipher new archives containing a long-term history of the surface evolution of the Sila upland plateau, Italy. This novel approach has shown that the exhumation rates of tors (as determined by surface exposure dating) give valuable insight into the temporal evolution of surface denudation and, thus, of soil erosion. Using the exposure age of tor surfaces, we were able to trace soil denudation and erosion over for the last 100 ka. Through the use of $^{239+240}\text{Pu}$, we were able to extrapolate the time series to the present. The correlation between $\delta^{13}\text{C}$ and total C_{org} did not provide any further, useful information about erosion.

We detected extremely low rates from MIS6/MIS5 (130–80 ka; Lisiecki, 2005) to the LGM (~21 ka), mostly below $30 \text{ t km}^{-2} \text{ year}^{-1}$ (about $0.036 \text{ mm year}^{-1}$). Over this period, continuous soil formation seemed to have occurred (progressive phase), also stimulated by a volcanic ash input from the Lipari Islands. However, soil erosion rates strongly increased at the transition from the Pleistocene to the Holocene, with the effect that total denudation rates were faster than soil production rates giving rise to a regressive phase of soil evolution. The rapid warming and accompanied increasing moisture at this time are a plausible cause for this. The strong increase in soil erosion during the Holocene and particularly during the last few decades is largely due to human impact. The $^{239+240}\text{Pu}$ data suggest soil erosion rates for the last five decades ($\geq 1,000 \text{ t km}^{-2} \text{ year}^{-1}$; about $1.22 \text{ mm year}^{-1}$) that are far above the natural rates of soil production. This will definitely lead to a distinct decrease in soil depth and with time to a landscape with shallower soils and rockier surface.

We showed that tors and boulders are a useful archive to reconstruct surface processes and soil erosion events. Together with Pu isotopes, this archive could be extended to the recent past and a relatively detailed chronology was obtained. Denudation processes could therefore be traced back from human to more geological timescales.

ACKNOWLEDGMENTS

This research was supported by the Swiss National Science Foundation (SNSF - Schweizerischer Nationalfonds zur Förderung der Wissenschaftlichen Forschung) project Grant 200021_162338/1. Special thanks go to Rahel Wanner of the ZHAW for the CHN measurements and Moritz Reisser for his help in the laboratory. Kevin Patrick Norton was supported by a SNSF Visiting International Fellowship (IZKOZ2_170715/1) and the Royal Society Te Apārangi Rutherford Discovery Fellowship. Fabio Scarciglia was supported by a SNSF grant for a Short Research Visit (IZKOZ2_147421). Finally, we thank three anonymous reviewers and Kristina Hippe for their constructive suggestions.

ORCID

Gerald Raab  <http://orcid.org/0000-0002-3063-6806>

REFERENCES

- Alewell, C., Egli, M., & Meusburger, K. (2015). An attempt to estimate tolerable soil erosion rates by matching soil formation with denudation in Alpine grasslands. *Journal of Soils and Sediments*, 15(6), 1383–1399. <https://doi.org/10.1007/s11368-014-0920-6>
- Alewell, C., Meusburger, K., Juretzko, G., Mabit, L., & Ketterer, M. E. (2014). Suitability of $^{239+240}\text{Pu}$ and ^{137}Cs as tracers for soil erosion assessment in mountain grasslands. *Chemosphere*, 103, 274–280. <https://doi.org/10.1016/j.chemosphere.2013.12.016>
- Alewell, C., Pitois, A., Meusburger, K., Ketterer, M., & Mabit, L. (2017). $^{239+240}\text{Pu}$ from “contaminant” to soil erosion tracer: Where do we stand?. *Earth-Science Reviews*, 172, 107–123. <https://doi.org/10.1016/j.earscirev.2017.07.009>
- Allen, J. R. M., Brandt, U., Brauer, A., Hubberten, H. W., Huntley, B., Keller, J., ... Zolitschka, B. (1999). Rapid environmental changes in southern Europe during the last glacial period. *Nature*, 400, 740–743. <https://doi.org/10.1038/23432>
- Allen, J. R. M., Watts, W. A., McGee, E., & Huntley, B. (2002). Holocene environmental variability – the record from Lago Grande di Monticchio, Italy. *Quaternary International*, 88, 69–80. [https://doi.org/10.1016/S1040-6182\(01\)00074-X](https://doi.org/10.1016/S1040-6182(01)00074-X)
- Amato, A., Aucelli, P. P. C., & Cinque, A. (2003). The long-term denudation rate in the Southern Apennines Chain (Italy): A GIS-aided estimation of the rock volumes eroded since middle Pleistocene time. *Quaternary International*, 101–102, 3–11. [https://doi.org/10.1016/S1040-6182\(02\)00087-3](https://doi.org/10.1016/S1040-6182(02)00087-3)
- Anderson, S. P., Dietrich, W. E., & Brimhall, G. H. (2002). Weathering profiles, mass-balance analysis, and rates of solute loss: Linkages between weathering and erosion in a small, steep catchment. *Geological Society of America Bulletin*, 114(9), 1143–1158. [https://doi.org/10.1130/0016-7606\(2002\)114<1143:WPMBAA>2.0.CO;2](https://doi.org/10.1130/0016-7606(2002)114<1143:WPMBAA>2.0.CO;2)
- Bajard, M., Poulencq, J., Sabatier, P., Develle, A. L., Giguët-Covex, C., Jacob, J., ... Arnaud, F. (2017). Progressive and regressive soil evolution phases in the Anthropocene. *Catena*, 150, 39–52. <https://doi.org/10.1016/j.catena.2016.11.001>
- Balco, G., Stone, J. O., Lifton, N. A., & Dunai, T. J. (2008). A complete and easily accessible means of calculating surface exposure ages or erosion rates from ^{10}Be and ^{26}Al measurements. *Quaternary Geochronology*, 8, 174–195. <https://doi.org/10.1016/j.quageo.2007.12.001>
- Bartley, R., Croke, J., Brainbridge, Z. T., Austin, J. M., & Kuhnert, P. M. (2015). Combining contemporary and long-term erosion rates to target erosion hot-spots in the Great Barrier Reef, Australia. *Anthropocene*, 10(1–2), 1–12. <https://doi.org/10.1016/j.ancene.2015.08.002>
- Bellin, N., Vanacker, N., & Kubik, P. W. (2014). Denudation rates and tectonic geomorphology of the Spanish Betic Cordillera. *Earth and Planetary Science Letters*, 390, 19–30. <https://doi.org/10.1016/j.epsl.2013.12.045>
- Bierman, P. R., & Caffee, M. (2001). Slow rates of rock surface erosion and sediment production across the Namib Desert and escarpment, Southern Africa. *American Journal of Science*, 301(4–5), 326–358. <https://doi.org/10.2475/ajs.301.4-5.326>
- von Blanckenburg, F., Belshaw, N. S., & O’Nions, R. K. (1996). Separation of ^9Be and cosmogenic ^{10}Be from environmental materials and SIMS isotope dilution analysis. *Chemical Geology*, 129, 93–99. [https://doi.org/10.1016/0009-2541\(95\)00157-3](https://doi.org/10.1016/0009-2541(95)00157-3)
- Boardman, J., & Poesen, J. (2007). *Soil erosion in Europe*. Chichester: John Wiley & Sons Ltd. <https://doi.org/10.1002/0470859202>
- Borchers, B., Marrero, S., Balco, G., Caffee, M., Goehring, B., Lifton, N., ... Stone, J. (2016). Geological calibration of spallation production rates in the CRONUS-Earth project. *Quaternary Geochronology*, 31, 188–198. <https://doi.org/10.1016/j.quageo.2015.01.009>
- Brown, E. T., Edmond, J. M., Raisbeck, G. M., Yiou, F., & Desgarceaux, S. (1992). Effective attenuation length of cosmic rays producing ^{10}Be and ^{26}Al in quartz: Implications for surface exposure dating. *Geophysical Research Letters*, 9, 369–372. <https://doi.org/10.1029/92GL00266>

- Bunzel, K., Kracke, W., & Schimmak, W. (1995). Migration of fallout $^{239+240}\text{Pu}$, ^{241}Am and ^{137}Cs in the various horizons of a forest soil under pine. *Journal of Environmental Radioactivity*, 28, 17–34. [https://doi.org/10.1016/0265-931X\(94\)00066-6](https://doi.org/10.1016/0265-931X(94)00066-6)
- Cacho, I., Grimalt, J. O., Canals, M., Sbaiffi, L., Shackleton, N. J., Schönfeld, J., & Zahn, R. (2001). Variability of the western Mediterranean Sea surface temperature during the last 25,000 years and its connection with the Northern Hemisphere climatic changes. *Paléo*, 16, 40–52. <https://doi.org/10.1029/2000PA000502>
- Chmeleff, J., von Blanckenburg, F., Kossert, K., & Jakob, D. (2010). Determination of the ^{10}Be half-life by multicollector ICP-MS and liquid scintillation counting. *Nuclear Instruments and Methods in Physics Research Section B: Beam Interaction with Materials and Atoms*, 268, 192–199. <https://doi.org/10.1016/j.nimb.2009.09.012>
- Christl, M., Vockenhuber, C., Kubik, P. Q., Wacker, L., Lachner, J., Alfimov, V., & Synal, H. A. (2013). The ETH Zurich AMS facilities: Performance parameters and reference materials. *Nuclear Instruments and Methods in Physics Research B*, 294, 29–38. <https://doi.org/10.1016/j.nimb.2012.03.004>
- Clift, P. D., Wan, S., & Blusztajn, J. (2014). Reconstructing chemical weathering, physical erosion and monsoon intensity since 25 Ma in the northern South China Sea: A review of competing proxies. *Earth Science Reviews*, 130, 86–102. <https://doi.org/10.1016/j.earscirev.2014.01.002>
- Conforti, M., Buttafuoco, G., Leone, A. P., Aucelli, P. P. C., Robustelli, G., & Scarciglia, F. (2013). Studying the relationship between water-induced soil erosion and soil organic matter using Vis-NIR spectroscopy and geomorphological analysis: A case study in southern Italy. *Catena*, 110, 44–58. <https://doi.org/10.1016/j.catena.2013.06.013>
- Darmody, R. G., Thorn, C. E., Seppälä, M., Campbell, S. W., Li, Y. K., & Harbor, J. (2008). Age and weathering status of granite tors in Arctic Finland (~68°N). *Geomorphology*, 94, 10–23. <https://doi.org/10.1016/j.geomorph.2007.04.006>
- van der Knijff JM, Jones RJA, Montanarella L. (1999). Soil erosion risk assessment in Italy. European Soil Bureau. EUR 19044 EN.
- van der Knijff JM, Jones RJA, Montanarella L. (2000). Soil erosion risk assessment in Europe. European Soil Bureau. EUR 19044 EN.
- Dixon, J. L., & von Blanckenburg, F. (2012). Soils as pacemakers and limiters of global silicate weathering. *Comptes Rendus Geoscience*, 344(11), 597–609. <https://doi.org/10.1016/j.crte.2012.10.012>
- Egli, M., Mirabella, A., Nater, M., Alioth, L., & Raimondi, S. (2008). Clay minerals, oxyhydroxide formation, element leaching and humus development in volcanic soils. *Geoderma*, 143, 101–114. <https://doi.org/10.1016/j.geoderma.2007.10.020>
- Egli, M., Norton, K., & Dahms, D. (2014). Soil formation rates on silicate parent material in alpine environments: Different approaches—different results? *Geoderma*, 213, 320–333. <https://doi.org/10.1016/j.geoderma.2013.08.016>
- Egli, M., & Poulencard, J. (2016). Soils of mountainous landscapes. In *International Encyclopedia of Geography: People, the Earth, Environment and Technology*, 1–10. <https://doi.org/10.1002/9781118786352.wbieg0197>
- von Eynatten, H., Tolosana-Delgado, R., Karius, V., Bachmann, K., & Caracciolo, K. (2015). Sediment generation in humid Mediterranean setting: Grain-size and source-rock control on sediment geochemistry and mineralogy (Sila Massif, Calabria). *Sedimentary Geology*, 336, 68–80. <https://doi.org/10.1016/j.sedgeo.2015.10.008>
- Frielinghaus, M., & Vahrson, W. G. (1998). Soil translocation by water erosion from agricultural cropland into wet depressions (morainic kettle holes). *Soil and Tillage Research*, 46, 23–30. [https://doi.org/10.1016/S0167-1987\(98\)80104-9](https://doi.org/10.1016/S0167-1987(98)80104-9)
- Gioia, D., Martino, C., & Schiattarella, M. (2011). Long- to short-term denudation rates in the southern Apennines: Geomorphological markers and chronological constraints. *Geologica Carpathica*, 62(1), 27–41. <https://doi.org/10.2478/v10096-011-0003-1>
- Google Earth. (2017). Version 7.3.2.5491 (July 10, 2017). Calabria Italy: Sila Massif.
- Google Maps. (2017). Retrieved from <https://www.google.com/maps/@39.3261099,16.527087,11.57z>
- Gosse, J. C., & Phillips, F. M. (2001). Terrestrial in situ produced cosmogenic nuclides: Theory and application. *Quaternary Science Reviews*, 20, 1475–1560. [https://doi.org/10.1016/S0277-3791\(00\)00171-2](https://doi.org/10.1016/S0277-3791(00)00171-2)
- Gunnell, Y., Jarman, D., Braucher, R., Calvet, M., Delmas, M., Leanni, L., ... Keddaouche, K. (2013). The granite tors of Dartmoor, Southwest England: Rapid and recent emergence revealed by Late Pleistocene cosmogenic apparent exposure ages. *Quaternary Science Reviews*, 61, 62–76. <https://doi.org/10.1016/j.quascirev.2012.11.005>
- Heimsath, A. M., Chappell, J., Dietrich, W. E., Nishiizumi, K., & Finkel, R. C. (2001). Late Quaternary erosion in southeastern Australia: A field example using cosmogenic nuclides. *Quaternary International*, 83, 169–185. [https://doi.org/10.1016/S1040-6182\(01\)00038-6](https://doi.org/10.1016/S1040-6182(01)00038-6)
- Hewawasam, T., von Blanckenburg, F., Schaller, M., & Kubik, P. W. (2003). Increase of human over natural erosion rates in tropical highlands constrained by cosmogenic nuclides. *Geology*, 31, 597–600. [https://doi.org/10.1130/0091-7613\(2003\)031<0597:IOHONE>2.0.CO;2](https://doi.org/10.1130/0091-7613(2003)031<0597:IOHONE>2.0.CO;2)
- Ibbeken, H., & Schleyer, R. (1991). *Source and sediment: A case study of provenance and mass balance at an active plate margin (Calabria, Southern Italy)*. Heidelberg: Springer. <https://doi.org/10.1007/978-3-642-76165-2>
- Johnson, D. L., & Watson-Stegner, D. (1987). Evolution model of pedogenesis. *Soil Science*, 143, 349–366.
- Kelly, J. M., Bond, L. A., & Beasley, T. M. (1999). Global distribution of Pu isotopes and ^{237}Np . *The Science of the Total Environment*, 237–238, 483–500. [https://doi.org/10.1016/S0048-9697\(99\)00160-6](https://doi.org/10.1016/S0048-9697(99)00160-6)
- Ketterer, M. E., Hafer, K. M., Link, C. L., Kolwaite, D., Wilson, J., & Mietelski, J. W. (2004). Resolving global versus local/regional Pu sources in the environment using sector ICP-MS. *Journal of Analytical Atomic Spectrometry*, 19, 241–245. <https://doi.org/10.1039/B302903D>
- Ketterer, M. E., Zhang, J., & Yamada, M. (2011). Application of transuranics as tracers and chronometers in the environment. In M. Baskaran (Ed.), *Handbook of environmental isotope geochemistry (Advances in Isotope Geochemistry)*. Heidelberg: Springer. DOI: 10.1007/978-3-642-10637-8
- Kirchner, J. W., Finkel, R. C., Riebe, C. S., Granger, D. E., Clayton, J. L., King, J. G., & Megahan, W. F. (2001). Mountain erosion over 10 yr, 10 ky, and 10 my time scales. *Geology*, 29(7), 591–594. [https://doi.org/10.1130/0091-7613\(2001\)029<0591:MEQYKY>2.0.CO;2](https://doi.org/10.1130/0091-7613(2001)029<0591:MEQYKY>2.0.CO;2)
- Kitchener, J. A. (1984). The froth flotation process: Past, present and future—in brief. In K. J. Ives (Ed.), *The scientific basis of flotation (Vol. 75) NATO ASI Series (Series E: Applied Sciences)*. Dordrecht: Springer. DOI: 10.1007/978-94-009-6926-1_2
- Kohl, C., & Nishiizumi, K. (1992). Chemical isolation of quartz for measurement of in-situ-produced cosmogenic nuclides. *Geochimica Cosmochimica Acta*, 56, 3583–3587. [https://doi.org/10.1016/0016-7037\(92\)90401-4](https://doi.org/10.1016/0016-7037(92)90401-4)
- Korschinek, G., Bergmaier, A., Faestermann, T., Gerstmann, U. C., & Rimmert, A. (2010). A new value for the half-life of ^{10}Be by heavy-ion elastic recoil detection and liquid scintillation counting. *Nuclear Instruments and Methods in Physics Research Section B: Beam Interaction with Materials and Atoms*, 268, 187–191. <https://doi.org/10.1016/j.nimb.2009.09.020>
- Kubik, P. W., & Christl, M. (2010). ^{10}Be and ^{26}Al measurements at the Zurich 6 MV Tandem AMS facility. *Nuclear Instruments and Methods B*, 268, 880–883. <https://doi.org/10.1016/j.nimb.2009.10.054>
- Lal, D. (1991). Cosmic ray labelling or erosion surfaces: In situ nuclide production rates and erosion models. *Earth and Planetary Science Letters*, 104, 424–439. [https://doi.org/10.1016/0012-821X\(91\)90220-C](https://doi.org/10.1016/0012-821X(91)90220-C)
- Lal, R., Tims, S. G., Fifield, L. K., Wasson, R. J., & Howe, D. (2013). Applicability of Pu-239 as a tracer for soil erosion in the wet-dry tropics of northern Australia. *Nuclear Instruments and Methods in Physics Research Section B*, 294, 577–583. <https://doi.org/10.1016/j.nimb.2012.07.041>

- Larsen, I. J., Almond, P. C., Eger, A., Stone, J. O., Montgomery, D. R., & Malcolm, B. (2014). Rapid soil production and weathering in the Western Alps, New Zealand. *Science*, 1244908. DOI: <https://doi.org/10.1126/science.1244908>, 637–640.
- Le Pera, E., & Sorriso-Valvo, M. (2000). Weathering and morphogenesis in a Mediterranean climate, Calabria, Italy. *Geomorphology*, 34(3), 251–270. [https://doi.org/10.1016/S0169-555X\(00\)00012-X](https://doi.org/10.1016/S0169-555X(00)00012-X)
- Lichter, J. (1998). Rates of weathering and chemical depletion in soils across a chronosequence of Lake Michigan sand dunes. *Geoderma*, 85, 255–282. [https://doi.org/10.1016/S0016-7061\(98\)00026-3](https://doi.org/10.1016/S0016-7061(98)00026-3)
- Liotta, D., Caggianelli, A., Kruhl, J. H., Festa, V., Prosser, G., & Langoe, A. (2008). Multiple injections of magmas along a Hercynian mid-crustal shear zone (Sila Massif, Calabria, Italy). *Journal of Structural Geology*, 30, 1202–1217. <https://doi.org/10.1016/j.jsg.2008.04.005>
- Lisiecki, L. E., & Raymo, M. E. (2005). A Pliocene-Pleistocene stack of 57 globally distributed benthic $\delta^{18}\text{O}$ records. *Paleoceanography*, 20, PA1003. <https://doi.org/10.1029/2004PA001071>
- Martino, C., Nico, G., & Schiattarella, M. (2009). Quantitative analysis of InSAR digital elevation models for identification of areas with different tectonic activity in southern Italy. *Earth Surface Processes and Landforms*, 34, 3–15. <https://doi.org/10.1002/esp.1681>
- McFadden, L. D. (2013). Strongly dust-influenced soils and what they tell us about landscape dynamics in vegetated arid lands of the southwestern United States. *Geological Society of America Special Papers*, 500, 501–532. [https://doi.org/10.1130/2013.2500\(15\)](https://doi.org/10.1130/2013.2500(15))
- Meusburger, K., Mabit, L., Ketterer, M., Park, J. H., Sandor, T., Porto, P., & Alewell, C. (2016). A multi-radionuclide approach to evaluate the suitability of $^{239+240}\text{Pu}$ as soil erosion tracer. *Science of the Total Environment*, 566, 1489–1499. <https://doi.org/10.1016/j.scitotenv.2016.06.035>
- Migoń, P. (2013). Weathering and hillslope development. In J. F. Shroder (Ed.), *Treatise on geomorphology* (Vol. 4) (pp. 159–178). San Diego: Academic Press. <https://doi.org/10.1016/B978-0-12-374739-6.00075-0>
- Molin, P., Pazzaglia, F. J., & Dramis, F. (2004). Geomorphic expression of active tectonics in a rapidly-deforming fore-arc, Sila Massif, Calabria, Southern Italy. *American Journal of Science*, 304, 559–589. <https://doi.org/10.2475/ajs.304.7.559>
- Moser, D., Di Pasquale, G., Scarciglia, F., & Nelle, O. (2017). Holocene mountain forest changes in central Mediterranean: Soil charcoal data from the Sila Massif (Calabria, southern Italy). *Quaternary International*, 457, 113–130. <https://doi.org/10.1016/j.quaint.2017.01.042>
- Mourier, B., Poulencard, J., Carcaillet, C., & Williamson, D. (2010). Soil evolution and subalpine ecosystem changes in the French Alps inferred from geochemical analysis of lacustrine sediments. *Journal of Paleolimnology*, 44(2), 571–587. <https://doi.org/10.1007/s10933-010-9438-0>
- Nishiizumi, K., Imamura, M., Caffee, M. W., Southon, J. R., Finkel, R. C., & McAnich, J. (2007). Absolute calibration of ^{10}Be AMS standards. *Nuclear Instruments & Methods in Physics Research Section B-Beam Interactions with Materials and Atoms*, 258, 403–413. <https://doi.org/10.1016/j.nimb.2007.01.297>
- Olivetti, V., Cyr, A. J., Molin, P., Faccenna, C., & Granger, D. E. (2012). Uplift history of the Sila Massif, southern Italy, deciphered from cosmogenic ^{10}Be erosion rates and river longitudinal profile analysis. *Tectonics*, 31, 1–19. <https://doi.org/10.1029/2011TC003037>
- Pelle, T., Scarciglia, F., Di Pasquale, G., Allevato, E., Marino, D., Robustelli, G., ... Pulice, I. (2013). Multidisciplinary study of Holocene archaeological soils in an upland Mediterranean site: Natural versus anthropogenic environmental changes at Cecita Lake, Calabria, Italy. *Quaternary International*, 303, 163–179. <https://doi.org/10.1016/j.quaint.2013.04.003>
- Pérez-Obiol, R., & Sadori, L. (2007). Similarities and dissimilarities, synchronisms and diachronisms in the Holocene vegetation history of the Balearic Islands and Sicily. *Vegetation History and Archaeobotany*, 16(4), 259–265. <https://doi.org/10.1007/s00334-006-0038-x>
- Portes, R., Dahms, D., Brandová, D., Raab, G., Christl, M., Kühn, P., ... Egli, M. (2018). Evolution of soil erosion rates in alpine soils of the Central Rocky Mountains using fallout Pu and $\delta^{13}\text{C}$. *Planetary Science Letters*, 496, 258–269. <https://doi.org/10.1016/j.epsl.2018.06.002>
- Pimentel, D. (2006). Soil erosion: A food and environmental threat. *Environment, Development and Sustainability*, 8(1), 119–137. <https://doi.org/10.1016/j.epsl.2004.07.031>
- Poesen, J. (2018). Soil erosion in the Anthropocene: Research needs. *Earth Surface Processes and Landforms*, 43, 64–84. <https://doi.org/10.1002/esp.4250>
- Raab, G., Halpern, D., Scarciglia, F., Raimondi, S., Norton, K., Pettke, T., ... Egli, M. (2017). Linking tephrochronology and soil characteristics in the Sila and Nebrodi mountains, Italy. *Catena*, 158, 266–285. <https://doi.org/10.1016/j.catena.2017.07.008>
- Reeves, D., & Rothman, D. H. (2014). Diffusion and kinetic control of weathering layer development. *Geofluids*, 14, 128–142. <https://doi.org/10.1111/gfl.12056>
- Rossetti, F., Faccenna, C., Goffé, B., Monié, P., Argentieri, A., Funicello, R., & Mattei, M. (2001). Alpine structural and metamorphic signature of the Sila Piccola Massif nappe stack (Calabria, Italy): Insights for the tectonic evolution of the Calabrian Arc. *Tectonics*, 20, 112–133. <https://doi.org/10.1029/2000TC900027>
- Scarciglia, F. (2015). Weathering and exhumation history of the Sila upland plateaus, southern Italy: A geomorphological and pedological perspective. *Journal of Soils and Sediments*, 15, 1278–1291. <https://doi.org/10.1007/s11368-014-0923-3>
- Scarciglia, F., Critelli, S., Borrelli, L., Coniglio, S., Muto, F., & Perri, F. (2016). Weathering profiles in granitoid rocks of the Sila Massif uplands, Calabria, southern Italy: New insights into their formation process and rates. *Sedimentary Geology*, 336, 46–67. <https://doi.org/10.1016/j.sedgeo.2016.01.015>
- Scarciglia, F., De Rosa, R., Vecchio, G., Apollaro, C., Robustelli, G., & Terrasi, F. (2008). Volcanic soil formation in Calabria (southern Italy): The Cecita Lake geosol in the late Quaternary geomorphological evolution of the Sila uplands. *Journal of Volcanology Geothermal Research*, 177, 101–117. <https://doi.org/10.1016/j.jvolgeores.2007.10.014>
- Scarciglia, F., Le Pera, E., & Critelli, S. (2005a). Weathering and pedogenesis in the Sila Grande Massif (Calabria, south Italy): From field scale to micromorphology. *Catena*, 61, 1–29. <https://doi.org/10.1016/j.catena.2005.02.001>
- Scarciglia, F., Le Pera, E., Vecchio, G., & Critelli, S. (2005b). The interplay of geomorphic processes and soil development in an upland environment, Calabria, South Italy. *Geomorphology*, 69, 169–190. <https://doi.org/10.1016/j.geomorph.2005.01.003>
- Schaller, M., Ehlers, T. A., Stor, T., Torrent, J., Lobato, L., Christl, M., & Vockenhuber, C. (2016). Spatial and temporal variations in denudation rates derived from cosmogenic nuclides in four European fluvial terrace sequences. *Geomorphology*, 274, 180–192. <https://doi.org/10.1016/j.geomorph.2016.08.018>
- Schaub, M., & Alewell, C. (2009). Stable carbon isotopes as an indicator for soil degradation in an alpine environment (Urseren Valley, Switzerland). *Rapid Communications Mass Spectrometry*, 23, 1499–1507. <https://doi.org/10.1002/rcm.4030>
- Smithson, P., Addison, K., & Atkinson, K. (2008). *Fundamentals of the physical environment: Fourth edition* (Vol. 65). (pp. 234–235). New York: Routledge. https://doi.org/10.1111/j.1745-7939.2009.01167_1.x
- Sommer, M., Gerke, H. H., & Deumlich, D. (2008). Modelling soil landscape genesis—A “time split” approach for hummocky agricultural landscapes. *Geoderma*, 145, 480–493. <https://doi.org/10.1026/j.geoderma.2008.01.012>
- Sorriso-Valvo, M. (1993). The geomorphology of Calabria. A sketch. *Geografia Fisica e Dinamica Quaternaria*, 16, 75–80.
- Spina, V., Galli, P., Tondi, M., Critelli, S., & Cello, G. (2007). Kinematics and structural properties of an active fault zone in the Sila Massif (Northern Calabria, Italy). *Bollettino Della Società Geologica Italiana*, 126, 427–438.
- Stone, J. O. (2000). Air pressure and cosmogenic isotope production. *Journal of Geophysical Research*, 105, 753–759. <https://doi.org/10.1029/2000JB900181>

- Tinner, W., van Leeuwen, J. F. N., Colombaroli, D., Vescovi, E., van der Knapp, W. O., Henne, D. P., ... La Mantia, T. (2009). Holocene environmental and climatic changes at Gorgo Basso, a coastal lake in southern Sicily, Italy. *Quaternary Science Reviews*, 28, 1498–1510. <https://doi.org/10.1016/j.quascirev.2009.02.001>
- Twidale, C. R. (2002). The two-stage concept of landform and landscape development involving etching: Origin, development and implications of an idea. *Earth-Science Reviews*, 57(1–2), 37–74. [https://doi.org/10.1016/S0012-8252\(01\)00059-9](https://doi.org/10.1016/S0012-8252(01)00059-9)
- Ugolini, F. C., & Dahlgren, R. A. (2002). Soil development in volcanic ash. *Global Environmental Research*, 6(2), 69–82.
- Vanacker, V., Bellin, N., Molina, A., & Kubik, P. W. (2014). Erosion regulation as a function of human disturbances to vegetation cover: A conceptual model. *Landscape Ecology*, 29(2), 293–309. <https://doi.org/10.1007/s10980-013-9956-z>
- Vespasiano, G., Apollaro, C., De Rosa, R., Muto, F., Larosa, S., Fiebig, J., ... Marini, L. (2015). The Small Spring Method (SSM) for the definition of stable isotope–elevation relationships in northern Calabria (Southern Italy). *Applied Geochemistry*, 63, 333–346. <https://doi.org/10.1016/j.apgeochem.2015.10.001>
- Wakasa, S., Matsuzaki, H., Tanaka, Y., & Matsukura, Y. (2006). Estimation of episodic exfoliation rates of rock sheets on a granite dome in Korea from cosmogenic nuclide analysis. *Earth Surface Processes and Landforms*, 31, 1246–1256. <https://doi.org/10.1002/esp.1328>
- Wallbrink, P. J., & Murray, A. S. (1993). Use of fallout radionuclides as indicators of erosion processes. *Hydrological Processes*, 7, 297–304. <https://doi.org/10.1002/hyp.3360070307>
- Walling, D., & He, Q. (1999). Improved models for estimating soil erosion rates from cesium-137 measurements. *Journal of Environmental Quality*, 28, 611–622. <https://doi.org/10.2134/jeq1999.00472425002800020027x>
- Zanchetta, G., Borghini, A., Fallick, A. E., Bonadonna, F. P., & Leone, G. (2007). Late Quaternary palaeohydrology of Lake Pergusa (Sicily, southern Italy) as inferred by stable isotopes of lacustrine carbonates. *Journal of Palaeolimnology*, 38, 227–239. <https://doi.org/10.1007/s10933-006-9070-1>
- Zhang, X., Higgitt, D. L., & Walling, D. E. (1990). A preliminary assessment of the potential for using caesium-137 to estimate rates of soil erosion in the Loess Plateau of China. *Hydrological Science Journal*, 35, 43–252. <https://doi.org/10.1080/02626669009492427>
- Zollinger, B., Alewell, C., Kneisel, C., Meusburger, K., Brandová, D., Kubik, P., ... Egli, M. (2015). The effect of permafrost on time-split soil erosion using radionuclides (^{137}Cs , $^{239+240}\text{Pu}$, meteoric ^{10}Be) and stable isotopes ($\delta^{13}\text{C}$) in the eastern Swiss Alps. *Journal of Soils and Sediments*, 15(6), 1400–1419. <https://doi.org/10.1007/s11368-014-0881-9>

SUPPORTING INFORMATION

Additional supporting information may be found online in the Supporting Information section at the end of the article.

How to cite this article: Raab G, Scarciglia F, Norton K, et al. Denudation variability of the Sila Massif upland (Italy) from decades to millennia using ^{10}Be and $^{239+240}\text{Pu}$. *Land Degrad Dev*. 2018;1–17. <https://doi.org/10.1002/ldr.3120>